Polymer Artificial Muscles

Controls and Applications with Low-Cost Twist Insertion Fiber Actuators

A Major Qualifying Project

Submitted to the Faculty of Worcester Polytechnic Institute

in partial fulfillment of the requirements for the

Degree of Bachelor of Science in Robotics Engineering

By

William Hunt

Robotics Engineering Program

Date: 6 May 2015

Project Advisor:

Professor Cagdas Onal

Abstract

Functional artificial muscle fibers could reduce the cost, weight and complexity of many robotic systems, and are therefore an attractive development goal in robotics engineering. When coiled into flexible helical artificial muscle fibers, Nylon monofilaments produce linear tensile actuation under thermal stimulus. In this research the behavior of these coiled muscle fibers was investigated using a test fixture designed to emulate the conditions in a real application. Tests showed muscle performance consistent with past research, but also revealed a previously undocumented thermal effect wherein muscles changed length unexpectedly under variable-loading conditions at high temperatures. This effect, along with other known properties of the muscle fibers, was modeled in a parametric simulation environment, and parameter estimation utilities were used to quantitatively match the model to the real-world response. The matched parameter model was used to simulate a computer controlled antagonistic servo-joint, which illustrated the potential of the muscle fibers for real-world application, and the controls challenges introduced by the newly discovered thermal effect.

Acknowledgements

It is difficult to thoroughly document the network of exceptional individuals who maintain the world-class research environment at Worcester Polytechnic Institute. The author Mr. Hunt wishes to express particular gratitude for the continuing assistance of advisor Prof. Cagdas Onal, along with his doctoral research staff in the WPI Soft Robotics Laboratory. Special thanks are extended to Arthur C. Heinricher at WPI, for his ongoing encouragement and support of the author's work leading up to this project.

Additional thanks to:

E.A. Partlow III, Cornell University

R. Baughman, U.T. Dallas

Washburn Laboratories, WPI

T. Chaulk & J. Johnson, WPI

P. Radhakrishnan, WPI

Contents

1 INTRODUCTION

1.1 BASIS FOR THIS RESEARCH

There are a number of robotic applications for low-cost muscle-like actuators, especially in rapidly developing fields such as humanoid control, active prosthetic design and wearable textile devices [5]. Artificial muscle technologies could lead to an era of dramatically increased human-robot interaction and integration, wherein humans receive replacement artificial muscle implants, and robots become just as nimble and dexterous as their human designers [29].

Haines *et al*. have demonstrated a novel approach for synthesizing artificial muscle-like actuator fibers from commercially available, low-cost polymer fibers such as fishing line by twist insertion. These fibers exhibit contraction of up to 49%, with considerable load capacity and very low hysteresis. They offer cost, simplicity, weight and strength advantages over a number of existing technologies. In particular, they possess a high strength-to-weight ratio, making them potentially valuable in aerospace applications. Several example configurations for the application of these fibers have already been demonstrated, including textile-woven, braided, plied and bundled actuators, driven electro- and hydro-thermally [5].

This project investigates robotic design applications and limitations for the polymer muscle fibers of Haines *et al*. in research and development phases. First, elements of muscle fiber production are reproduced. Next, a prototype actuator configuration is developed, and used to perform an assay of non-repeatable elements in muscle actuation, and the resulting limitations on muscle control. Finally, a controlled model for a 1-DOF rotational robotic joint (based upon the prototype actuator configuration) is produced in-silico. The dynamical characteristics of this simulated joint are documented, and potential applications are discussed.

1.2 Contributions to the Field

This project attempts to recreate the helical muscle fibers of Haines *et al.*, characterize some of their behavioral properties, and demonstrate a prototype antagonistic rotary actuator configuration in-silico, using Joule heating and passive cooling. The end result and primary robotic design component of this project is a rotational joint fixture that can be driven by antagonistically biased (prestrained) muscle fibers, and which may be used by a future project group to implement the simulated joint from this project. This joint illustrates the applicability of twist-insertion fiber actuators to controlled robots, and reveals the limitations of the actuators. As such, this work also provides an outline for future research in soft robotic actuation systems, especially those that require high work capacity, including aerospace, micro- and nano-robots, and ultra-low-cost systems.

2 Background

2.1 Muscle Applications in Robotics

Many robotics applications require control of the position and/or dynamical characteristics of a mechanism. There is widespread interest in a category of actuators that behave similarly to natural muscle fibers, affording positional, force and/or impedance control while maintaining a flexible, lightweight form factor. Artificial muscle technologies are an attractive solution to challenging robotics problems, especially in robots such as humanoids, manipulators and prostheses [5]. Artificial muscles may also be useful in aerospace, as they provide a light-weight alternative to existing transducer technology. Contrary to traditional cost- and weight-expensive geared motors, artificial muscle systems have the potential to be both physically and operationally flexible, and customizable for a wide range of applications [29].

Pneumatic muscle systems are already known to be well suited for complicated open-chain robots [10]; these systems have been used in various robots including humanoid walking systems [19] and dexterous graspers [27]. Force application contexts that preclude more traditional actuators due to weight, noise or cost are good potential applications for pneumatic muscles. For example, Serres [16] showed an application for pneumatic muscles in human resistive strength training under orbital microgravity.

Natural muscles operate in antagonistic pairs or groups, which afford precise control of movement [1]. Human motion is dependent upon the dynamical characteristics of these muscle groups. Modern walking prostheses seek to emulate the properties of natural limbs, which can dynamically adjust mechanical joint impedance properties [11]. While existing systems such as hysteresis brakes and series elastic actuators allow this type of control, these technologies can be cumbersome and expensive. Artificial muscle systems may solve this problem in a more compact, comfortable package [11]. Developers of walking and humanoid robots have attempted to emulate the dynamical properties of natural muscle groups [18]. Artificial muscles are likely to improve the realism of these bio-mimetic designs,

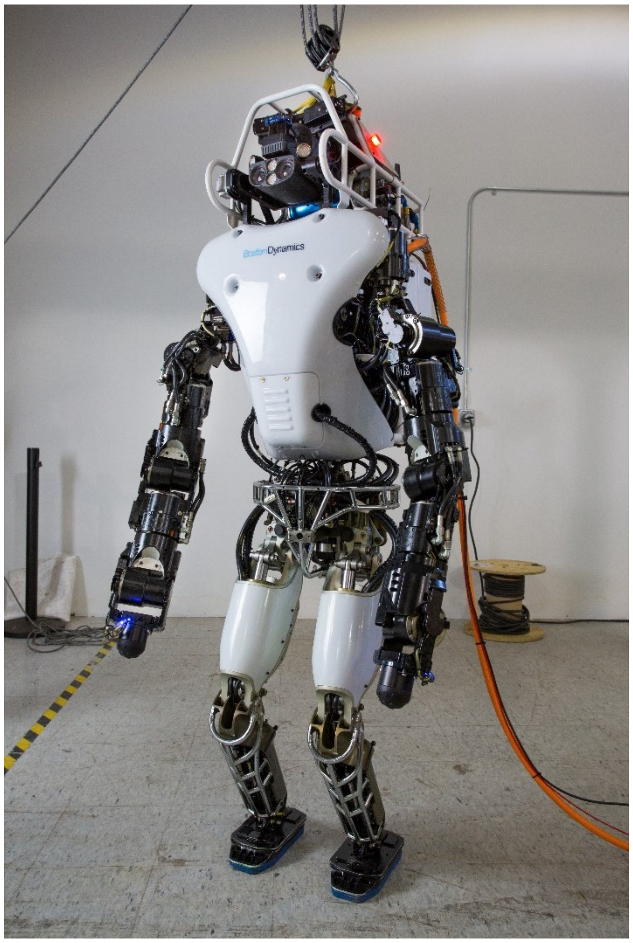
Fig. 1: Atlas, a modern humanoid robot, image credit WPI via DARPA [25]

because these actuators typically operate in antagonistic groups [10]. Complicated movements such as walking have already been achieved using this approach [19].

Artificial muscles have been applied in non-traditional applications. Madden *et al*. [14] provided case studies detailing naval-specific muscle applications for controlling the shape and orientation of propeller blades. An example variable-camber propeller was proposed for the Expendable, Mobile Antisubmarine Warfare Training Target (EMATT) vehicle, and some existing artificial muscle technologies were shown to be feasible actuation systems for this design [14]. Because of their light weight, artificial muscles could also be valuable in aerospace systems.

2.2 Past Work in Artificial Muscles

Artificial muscle research has spanned various technologies, many of which are based around specialized materials. In some cases, esoteric alloys, polymers and gels have been shown to exhibit muscle-like behavior. In other cases, more conventional materials and technologies have been formed into macroscopic structure that create the desired behavior. Artificial muscle research draws heavily on the findings of materials science and nanotechnology scholars.

Perhaps the most conventional and well-known artificial muscle technology is the pneumatic or McKibben air muscle [2]. A pneumatic muscle is constructed by containing an airtight, flexible tube or bladder within a braided, non-extensible fiber shell. When the bladder is inflated, the shell converts the inflating pressure into a compressive or tensile force along the length of the muscle, resulting in displacement and/or force

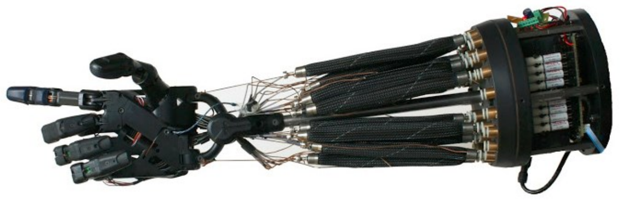
Fig. 2: Robotic hand using air muscles, image credit Shadow Robot Company [26]

application. These actuators are strong and light, but (like other fluidic actuators) they require pressure and valve systems [2].

As noted above, pneumatic muscles have seen significant adoption [10][19][27][16]. One application, a dexterous hand from the Shadow Robot Company, is shown in Fig. 2 [26]. Existing applications for pneumatic muscles may benefit from the introduction of more advanced muscle-like actuators that do not require fluidic control overhead.

Relatively common material-based artificial muscle technologies are based around shape memory alloys (SMAs), which include the well-known Nitinol (a nickel-titanium alloy). SMAs can be formed into muscle-like devices that actuate with temperature [13]. SMA products are commercialized and broadly available for muscle applications. An example product is Flexinol actuator wire, available from Dynalloy, Inc. [9]. Flexinol is a Nitinol variant, capable of up to 7% reversible stroke with a muscle strength that exceeds the yield strength of the alloy at operating temperature (a Flexinol wire can exert enough force to break itself).

SMAs have convenient features such as intrinsic conductivity, which permits direct electrothermal heating. Unfortunately, while they can provide fast, high energy strokes, SMAs are highly hysteretic and therefore difficult to control [5][13]. SMAs are also expensive when used in large quantities to achieve high-strength actuation: the cost of Flexinol wire actuators exceeds $700 US per kilogram [8].

Shape Memory Polymers (SMPs) provide similar functionality to SMAs, but at a lower strength, cost and weight. They are not inherently conductive, so they are harder to heat than Nitinol and its variants [17]. Fiber reinforcement provides some improvement in SMP strength [17], and researchers showed that performance improved when SMPs were filled with carbon nanotubes [12].

Another polymer solution uses an electroactive approach, in which dielectric elastomers are subjected to electric fields [24]. This Electro-active Polymer (EAP) technology does not require heating for actuation, but necessitates a high voltage [5][24]. Some other electroactive polymers need to be stimulated chemically or electrochemically, in a wet environment, or are themselves gels [11]. These technologies have exhibited relatively high efficiencies (~20%), but impose the additional system load of chemical storage and delivery [11].

Carbon nanotubes (CNTs) can be spun into yarns, which provide torsional and linear actuation under appropriate conditions [15][20]. These types of actuation can be induced by multiple stimulation methods, including electrochemical charge injection [15], gas absorption on an attached layer of palladium and thermal changes [20]. Thermal actuation was achieved by infiltrating the CNT yarn with a guest such as wax. When made to expand and contract under changes in temperature (which can be produced using light or electricity), wax-infiltrated yarns provided lengthwise actuation on the order of 5%, with a unit-mass work capacity up to 29 times that of a natural muscle [20]. Unfortunately these muscles rely on state-of-the-art carbon nanotube technology and are therefore expensive [5].

2.3 Twist-Insertion Polymer Muscles

Recent work by Haines *et al.* demonstrated a novel form for a thermo-mechanical artificial muscle based on low-cost, readily available precursor materials. The seminal work in *Science* [5] explained a process of twist insertion into drawn fibers of nylon (and similar materials).

When the twisted fibers are heated, they untwist, producing strong torsional actuation. If these same fibers are coiled into helical spring-like strands (as shown in Fig. 3), heating induces linear contraction along the helix axis. Haines *et al*. provided an overview of the characteristics of these actuator strands, and illustrated various example configurations including parallel linear actuators, braids and textiles. Twist insertion actuators have a work capacity, relative to mass, over 100 times that of natural human muscle [5], which is a three-fold improvement over the expensive carbon nanotube technology discussed above [20]. The coiled fibers exhibited very low hysteresis performance and sustained one million cycles of operation, but exhibited low maximum energy conversion efficiencies on the order of 1% [5].

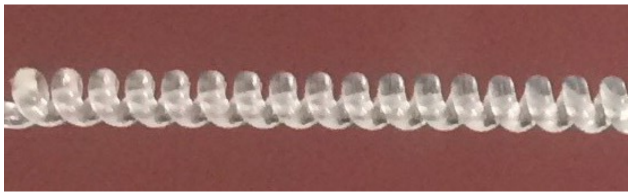
Fig. 3: Optical image of coiled nylon fiber actuator

In the original research, electro-thermal actuation was obtained using Joule heating in filaments pre-coated with conductive material, or by twisting a discrete conductive element into the fiber during fabrication. Hydro-thermal heating was also achieved by containing muscle fibers within a fluid-tight tube, which was alternately filled with hot and cold water to cycle the muscle [5]. In more recent research, fibers were painted with conductive silver paint before coiling. The silver paint then provided the electrical pathway for Joule heating. These silver-plated filament actuators cycled more quickly when cooled passively in water [25].

In some of the tests of Haines *et al.*, coiling was induced by continuous twisting of the fiber, to the point that the fiber began to twist around itself helically (a phenomenon known as writhe). In other tests, twisted fibers were wrapped around mandrels of various diameters. This produced muscles capable of greater actuation distance, but lower load capacity, a geometrically intuitive result [5].

Twist insertion muscles are extremely easy to manufacture, requiring only a rotating spindle and a means to keep the coiling fiber under tension. Media coverage of this technology has highlighted the ease of manufacturing from common fibers such as fishing line and sewing monofilament, and even encouraged hobbyists to pursue their own applications [6].

2.4 Twist Mechanics and Anisotropism

Haines *et al*. describe the thermal expansion of drawn polymer fibers, which can be anisotropic (an important property if mechanical twisting action is required) [5]. Aligned crystalline regions of polymer samples have negative thermal expansion along the chain direction, due to a hypothesized change in the rotation of carbon-carbon bonds within the polymer backbone [30]. Drawn fibers that are not entirely crystalline can exhibit a much greater lengthwise contraction than purely aligned crystalline molecules, because of the contraction of amorphous elastic tie molecules within the fiber structure [4][3]. These drawn fibers also expand diametrically, due to the expansion of crystalline regions [25][4]. The result is an anisotropic expansion, with a negative coefficient in the draw direction and a positive coefficient perpendicular thereto.

Torsional untwisting occurs when twisted polymers that exhibit these anisotropic expansion conditions are heated. When a fiber is twisted, the polymer chains oriented lengthwise along the fiber form helices. Shrinking in polymer chains now occurs along these helices. Haines *et al*. describe an analogous relationship between original fiber length, twist, axial length and diameter in the surface layer of a yarn [4]:

$$\frac{\Delta n}{n} = \frac{\Delta \lambda}{\lambda}\frac{1}{\cos^2 \alpha_f} - \frac{\Delta d}{d} - \frac{\Delta l}{l}\tan^2 \alpha_f \qquad \textbf{(1)}$$

In this expression, n is the fiber twist, λ the polymer chain length, l the twisted fiber length, α_f the angle of the molecular helix formed by twisting, d the original fiber diameter, and Δ-expressions the temperature-induced changes in these quantities. By this analogy, Haines *et al.* explained that a change in twist is related to lengthwise fiber contraction and diametric fiber expansion. As equation (1) illustrates, these two effects combine additively to affect torsional action. This leads to a useful conjecture: it is advantageous in twist-insertion muscle design to select precursor fibers with highly anisotropic thermal expansion characteristics, in which a temperature increase causes the fiber to contract lengthwise and expand diametrically [5][4].

2.5 Achieving Linear Actuation

The linear actuation achieved by helical fiber configurations is explained by the fiber untwisting effect described in the previous section. A fiber that has been coiled into a helix will undergo twisting when the helix is extended and compressed. The magnitude of this twisting is described by this equation, from Haines *et al.* [5]:

$$\Delta T = \frac{N\Delta L}{l^2} \qquad \textbf{(2)}$$

Where l is the length of the original, fiber, ΔL is the change in length of the helical coil, N is the number of coils and ΔT is the change in twist per unit length in the original fiber. Equation (2) is fundamentally a formulation of spring mechanics [5][25][4]; it illustrates that a change in fiber twist will produce a corresponding, proportional change in helix length. By comparison of the mechanical work achieved by torsional and linear twist-insertion actuators, Haines *et al.* demonstrated empirically that the twist-length relationship of equation (2) is likely to be the mechanism that drives linear actuation in coiled muscle fibers [5].

3 METHODS

3.1 METHOD OF FIBER GENERATION

A simple test and manufacturing fixture was developed to produce and characterize the twist insertion muscle fibers investigated by Haines *et al.* [5]. The twisting fixture comprised a benchtop twisting stand, a heat gun for muscle stimulation, and a digital camera for recording tests. The stand provided a convenient USB serial port user interface, controlled twist insertion, and a weight hook for gravitational tension application. Bags of small ball bearings, measured on scales, served as calibrated weights. Fig. 4 shows the fiber twisting and test stand CAD model.

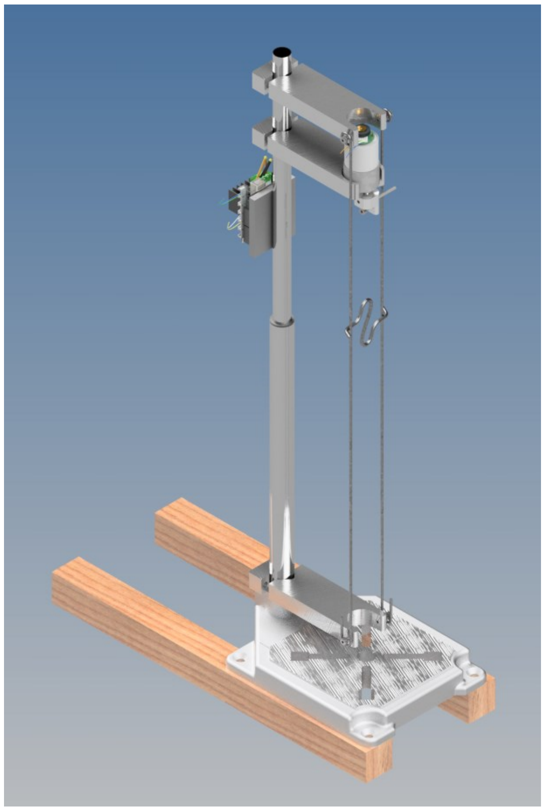
Fig. 4: Computer-aided design graphic for muscle twisting fixture

The tabletop test stand was only capable of twisting short lengths of muscle fiber, and could not twist muscles quickly. Thus, this fixture was dismantled for parts midway through the project period, and replaced by a less formal setup permitting rapid preparation of longer samples. A metal wire hook was installed in the chuck of a handheld electric drill. Nylon fiber tied to this hook was weighted to calibrated tensions by the same technique used for short lengths (a metal hook with a bag of weighted ball bearings). Longer fibers were coiled using existing vertical drops such as balconies and stairwells. For such large sample lengths, zip ties were attached to the weighted end of the twisting fiber and permitted to ride against a vertical wall or board to prevent unwinding.

To prevent muscles from uncoiling during transfer between the drill setup and test fixture, two-ply muscle fibers were produced using the technique detailed by Mirvakili *et al.* [25], namely grasping the center of the finished muscle coil and reducing muscle tension to create a snarl, which naturally nucleates a two-ply yarn. To terminate the two ply yarn, a short length of aluminum tubing was placed over the yarn product and crimped using pliers at a measured distance from the end of the fiber (see Fig. 5).

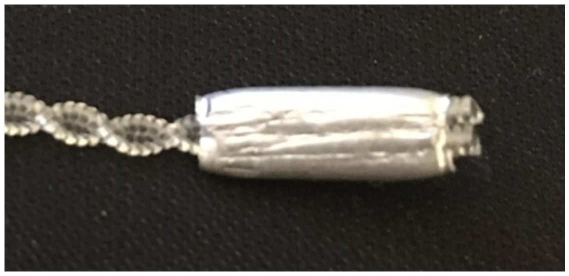
Fig. 5: Crimped aluminum tube on end of two-ply muscle

3.2 Preliminary Characterizations

The seminal research [5] illustrated that a wide range of spring indices could be achieved in the test fiber by nucleating coils at a common load and subsequently changing to a smaller or larger load, depending on the spring index desired. To reduce the number of variables at play and simplify the twist insertion process, this research addressed only artificial muscle fibers produced using a fixed load. Fiber characterization testing began with a series of coiling operations using a few different fiber diameters and coiling loads, to establish the range of loads that nucleated suitable coils in different diameter fibers.

Note that only a small selection of precursors was considered during this test, due to limitations on time for testing. The preliminary tests addressed here were performed on muscles coiled from 2-lb, 12-lb and 20-lb grades of a single example precursor product: Trilene XL Smooth Casting monofilament fishing line. As noted in the seminal research [5], twisted nylon actuators seem to exhibit common scale-independent behaviors, so it is reasonable to expect that the effects observed here will also occur when alternative precursor test ratings are used.

The procedure for static characterization required a very simple setup. A muscle was coiled on the test rig of Fig. 4 and loaded with a mass of known weight. It was then brought to a high temperature using a heat gun, and allowed to cool. At each step of heating and cooling, the temperature of the muscle was verified using a thermocouple, and an image was captured. This process of cycling was repeated several times, to "train" the muscle. After that point, the muscle was brought to a series of different temperatures (controlled by manually changing the distance to the heat gun), and images were captures at each step. Finally, the images collected during the test were analyzed in the program *Kinovea*[1] to determine the length of the fiber at each test point.

Note that the process of cycling the muscle to a high temperature was only added after a failed attempt at characterization illustrated a "training" effect. Whenever the load changed, cycling to high temperatures caused permanent deformation that did not reverse during cooling. By repeatedly cycling the muscle to a high temperature, it was possible to illustrate a condition of repeatable actuation.

The earliest characterization tests revealed a complex training effect, which prevented a basic model of muscle behavior from being established. To produce a more model-suggestive dataset, it was necessary to perform more elaborate series of tests, here dubbed the "detailed characterization". Detailed characterization was split into two test sequences, referenced here as T1 and T2.

The preliminary tests used a heat gun as a heat source, requiring a great deal of user input and control. The heat gun test rig was extremely slow and provided poor quality data points due to its lack of precise thermal control. It was determined to be inadequate for detailed characterizations. To mitigate this problem, various electrical heating systems were explored.

If the muscle was wrapped in a fine resistive wire, and the wire heated by an electric current, the muscle would theoretically take on the temperature of the wire after a certain period. When tested practically, however, the hot wire always formed a knife-like cutting edge and sliced through the muscle. Even a small indentation in the muscle fiber surface would be enough to nucleate further splitting, so it is reasonable that the hot-wire approach was impractical. A

[1] http://www.kinovea.org/

similar effect was observed when a multi-fiber conductive thread element was used in place of the hot wire. While the conductive thread element provided more diffuse heat, it still localized heating enough to cut through the fiber.

Haines *et al.* [5] demonstrated a mode of uniform surface-layer heating using pre-plated silver fibers. Those precursor fibers were not obtained in time for testing. A similar technique of [5] dictated that the muscle be wrapped in forest-grown carbon nanotube sheet, which formed a flexible conductive layer. This was similarly impractical within the scope of this project.

Mirvakili *et al.* [25] demonstrated a technique for reproducing the surface-layer heaters of [5], in which a conductive silver bearing paint was applied to the muscle surface at some point during manufacturing. An advantage to this method is the ability to apply the paint at any stage; e.g. mid-twisting but before supercoiling (the preferred technique in [25]), which theoretically reduces the amount of flexibility required. The paint used in [25] was SPI Flash-Dry, a very expensive compound intended for electrically conductive sample mounting. As a less expensive substitute, a vial of Ted Pella, Inc. *Pelco* Conductive Silver Paint was obtained.

At first, the muscle was painted during the coiling process, just before supercoiling. The *Pelco* paint proved insufficiently flexible, incrementally flaking off the muscle fiber during supercoiling. Next the paint was experimentally applied *after* coiling, to the entire muscle coil structure, using a foam applicator pad. This produced an effective surface heating element, but that element soon flaked away during muscle operation. At this point, the paint technique was abandoned due to the high cost of silver paint samples. Further testing used a more complex, but less expensive, alternative. It is recommended that future experimenters attempt to obtain pre-plated precursor fibers or the proper SPI Flash-Dry paint compound, in order to reproduce the heating elements from [5] and/or [25].

The low-cost heating alternative comprised a small-diameter tubular diffuser device. The heater itself comprised an aluminum tube, wrapped in Kapton tape, and subsequently in Kanthal heating wire. The selected tube's diameter was just large enough to accommodate a test muscle. Tubes constructed from kitchen-grade aluminum foil were tested and shown to be effective, but solid aluminum tubes with a greater wall thickness were stronger and easier to re-use. This design produced a uniform heated environment for the muscle, at the cost of high-speed heating and cooling (the heater tube diffuser introduced a large amount of extra thermal mass).

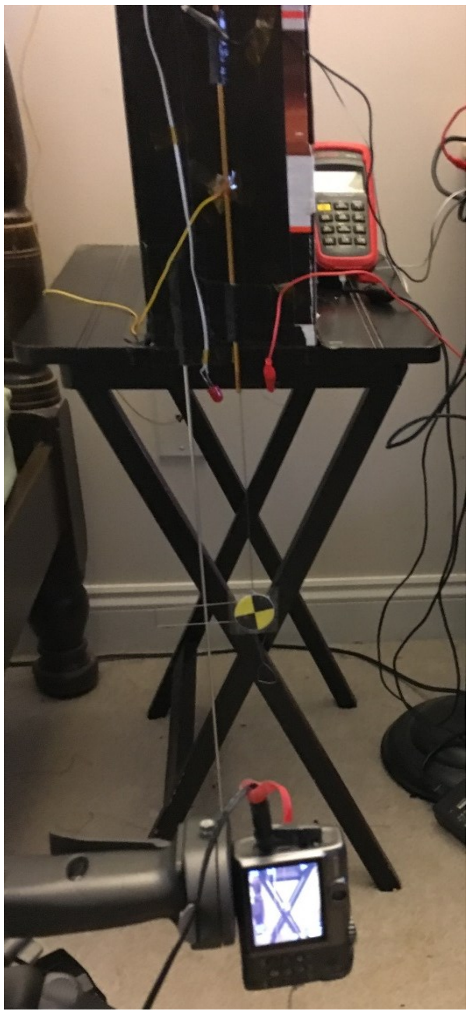
Fig. 6: Detail Test Setup

In the case of the preliminary tests, the tube was made long enough to completely contain the sample muscle fiber, Because the tube obscured the muscle's length and prevented direct weight attachment, a wire hanger was produced that fit inside of the tubular heater. This wire was attached to the end of the sample, and a weight hanger and anti-rotation moment arm were formed at the other end. Additionally, a circular vision target was affixed to the hanger, to simplify analysis of test images. An electrical current was applied to the Kanthal wire to increase the temperature of the muscle tube. An external, manually-controlled fan was sometimes used during cooling to speed up the tests.

The driver circuit for the heater was an older, single channel version of the circuit developed for the antagonistic test fixture, which is documented in Section 3.3. The original driver circuit was destroyed during transportation of the test setup, but the circuit for the antagonistic test fixture was designed to be compatible with the T1/T2 heater setup. Further documentation for that circuit is omitted here, as it is thoroughly documented in Section 3.3. Similarly, the computer program interface for the heater controller (a PI controller with a feedforward component) was very similar to that for the antagonistic fixture, also documented in Section 3.3. That program is omitted from this report, as it is merely an early version of the antagonistic fixture program, with slower logging and only a single channel of control. Note that this project did not use any source control repository or formal versioning, because the number of software tools developed was so small.

See Fig. 6 for a photograph of the test setup, and Fig. 7 for a photograph of the tube heater and hanger system.

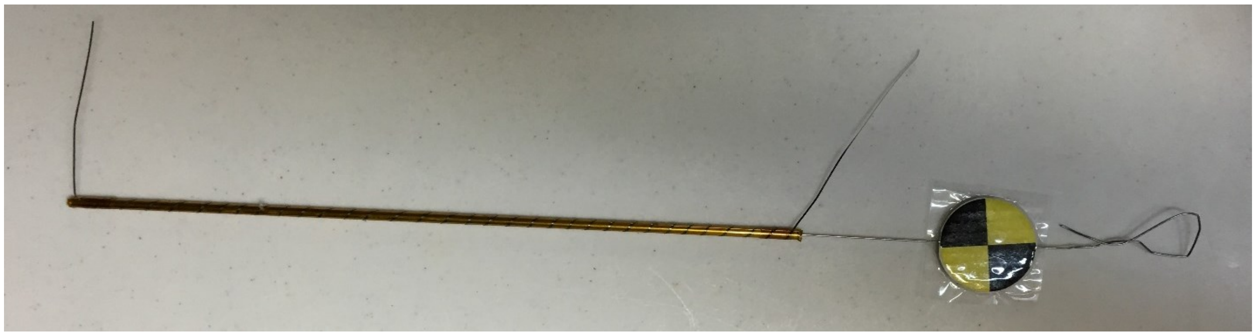

Fig. 7: Heater Tube and Hanger System

Detailed test T1 comprised a better controlled, more comprehensive version of the preliminary muscle test, with the goal of obtaining a constitutive equation accounting for the full regime of *repeatable* actuation available from the polymer muscle fiber. T1 did not attempt to characterize non-repeatable (plastic) phenomena.

A sample two-ply muscle was loaded into the heater tube, and a small weight of 275 g was applied. The heater was then cycled to a high temperature (90°C) and returned to room temperature (approximately 25°C) five times. After cycling, muscle fiber temperature was swept through a series of increasing values, and finally returned to room temperature. At this point, the load on the muscle was increased, and the process repeated.

This was the extent of testing performed in the preliminary phase. For T1, though, additional data points were collected; after the first batch of data, a series of five additional batches were collected. The procedures for these batches were identical, but in each new batch, the peak temperature used during initial cycling was reduced. In an attempt to prevent previous tests from influencing each new batch, the muscle was cycled five times to 90 degrees at the 275 g load between batches.

To communicate the basis for test T2, a brief digression into the results of T1 is necessary. T1 demonstrated that muscle actuation could be described using two quantities in superposition, first an actuation descriptor c, and second a deformation descriptor s. The actuation descriptor appeared to be an instantaneous function of muscle temperature, while the deformation s appeared to depend on the muscle's historical temperature and load parameters. In short, the parameter s accounted for plastic deformation and nonlinear dynamic effects.

Originally, test T2 was intended to produce a thorough characterization of the behavior of parameter s and therefore the hysteretic element of the muscle constitutive model. Unfortunately, time did not permit such a complete characterization. Instead, a slice of the sample space was collected using the following regime:

T2.i Cycle to a high temperature at a low load (90°C, 275 g).
T2.ii Cool to a low temperature (25°C, 275 g).

T2.iii Change load to a “starting load” parameter (25°C, starting load).
T2.iv Heat to a “starting temperature” parameter (starting temperature, starting load).
T2.v Cool to low temperature (25°C, starting load).
T2.vi Change to “ending load” parameter (25°C, ending load).
T2.vii Heat to “ending temperature” parameter (ending temperature, ending load).
T2.viii Heat to high temperature (90°C, ending load).
T2.ix Change load to low load (90°, 275 g).
T2.x Start over at step T2.ii with a new set of load and temperature parameters; repeat for various parameter permutations.

These tests were performed at a set of loads (700 g, 850 g, 1000 g, 1150 g) and temperatures (25°C, 50°C, 70°C, 90°C) in each available permutation of starting load, ending load, starting temperature, and ending temperature. Accounting for small amounts of data lost due to testing error, 250 of the available 256 permutations were successfully captured. The structure of these tests permitted deduction of the behavior of the *s* parameter during heating from room temperature, after training to many different sets of loads and temperatures.

Because the heating processes in T2 were only performed starting at room temperature, T2 did not generate a comprehensive constitutive equation for plastic deformation behavior. Complete tests would need to assess the effect of changing both temperature and load, without returning to room temperature in between events. Nevertheless, T2 illustrated the degree of plastic deformation possible during muscle operation within a wide range of temperatures, and was therefore informative of broad quantitative conclusions about muscle control and application limitations.

3.3 DESIGN OF ANTAGONISTIC CONFIGURATION

The antagonistic test configuration was designed to permit testing in a realistic use case, where the muscle under test drives a rotor whose position may be monitored. The configuration needed a rotor with attachment points at various radii, a stator with adjustable attachment points, and a low-resistance means for monitoring the position of the rotor. A final feature requirement was added to simplify the application of torque: a disc of constant radius from which a weight-bearing cable can be suspended, attached to the rotor and concentric with the axis of rotation.

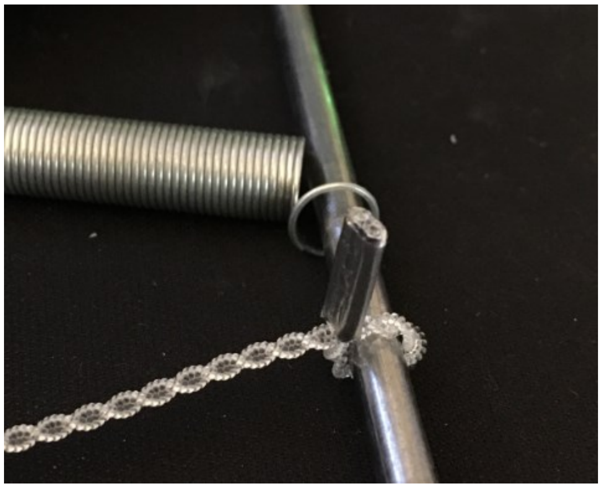
Fig. 8: Steel Pin with Attached Muscle and Spring

Both springs and muscles could be used as antagonistic force elements, in various configurations. The ends of two-ply muscles are easily looped through their own twists to form tightening loops. Extension springs also include loops for mounting. Thus, steel pins (as shown in Fig. 8) provided a convenient connection means for both these forms of stimulus. These pins could be easily supported by drilled holes, so a "pegboard" arrangement of mounting holes was included in the fixture to satisfy the requirement for adjustable mounting locations.

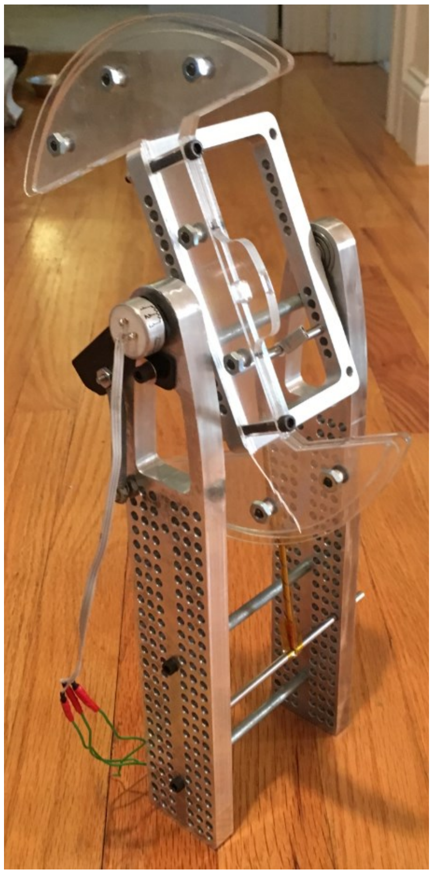
Fig. 9: Antagonistic Test Fixture

To measure the position of the rotor, a low friction Vishay Spectrol potentiometer was purchased. Rigid mounting of the potentiometer was not acceptable, as even the slightest misalignment of the shafts would introduce binding. Instead, a method similar to patent US 2937861 [23] was adapted to the design. The potentiometer was mounted to a plastic armature.

A small extension spring held the armature against a sliding contact surface. The potentiometer's shaft was coated in a small quantity of beeswax and pressed into a hole along the rotation axis of the rotor. As the rotor and potentiometer shaft rotated, the mounting armature provided counter-rotation torque on the body of the potentiometer, while allowing the potentiometer body to translate slightly, thereby avoiding a binding condition.

The finished fixture is shown in Fig. 9. For detailed design drawings of the components and assembly of the antagonistic configuration, see Appendix A.

To heat the muscles installed in the antagonistic fixture, tubular aluminum heaters were constructed with Kanthal heater wire. The heaters for the antagonistic joint fixture were shorter than the heater from the preliminary test (described in Section 3.2 and illustrated in Fig. 7) but otherwise identical in form and function. Because the antagonistic fixture design required the ends of the muscles to be exposed, the heater tubes were cut short and affixed at one end of the muscles using Kapton tape. This arrangement allowed the muscle fibers to move in and out of the heater tubes, complicating the mode of heating but permitting inflexible heater geometry.

The fixture required two computer-interfaced electrical subsystems to operate: a thermal control system, capable of heating and cooling two muscle heater channels and measuring their temperatures, and a position measurement system, capable of reading the state of the potentiometer. To speed up sampling, two independent Arduino serial interface boards were used, one for temperature control and another for sensor feedback. These interface boards were loaded with a remote prototyping API downloaded from the web[2] and modified for this custom use. An external computer was programmed in Python to command the boards, using a Python

[2] https://github.com/HashNuke/Python-Arduino-Prototyping-API

module provided by the remote prototyping API and modified for this custom use. Note that the Arduino Prototyping API was used freely under the MIT License.

Temperature measurement was accomplished using an Amprobe TMD-56 thermocouple meter with two K-type thermocouples. An interpreter program for the USB interface on the TMD-56, taken from the open source project *Artisan* on GitHub[3], was modified to permit access to the temperature reading inside Python.

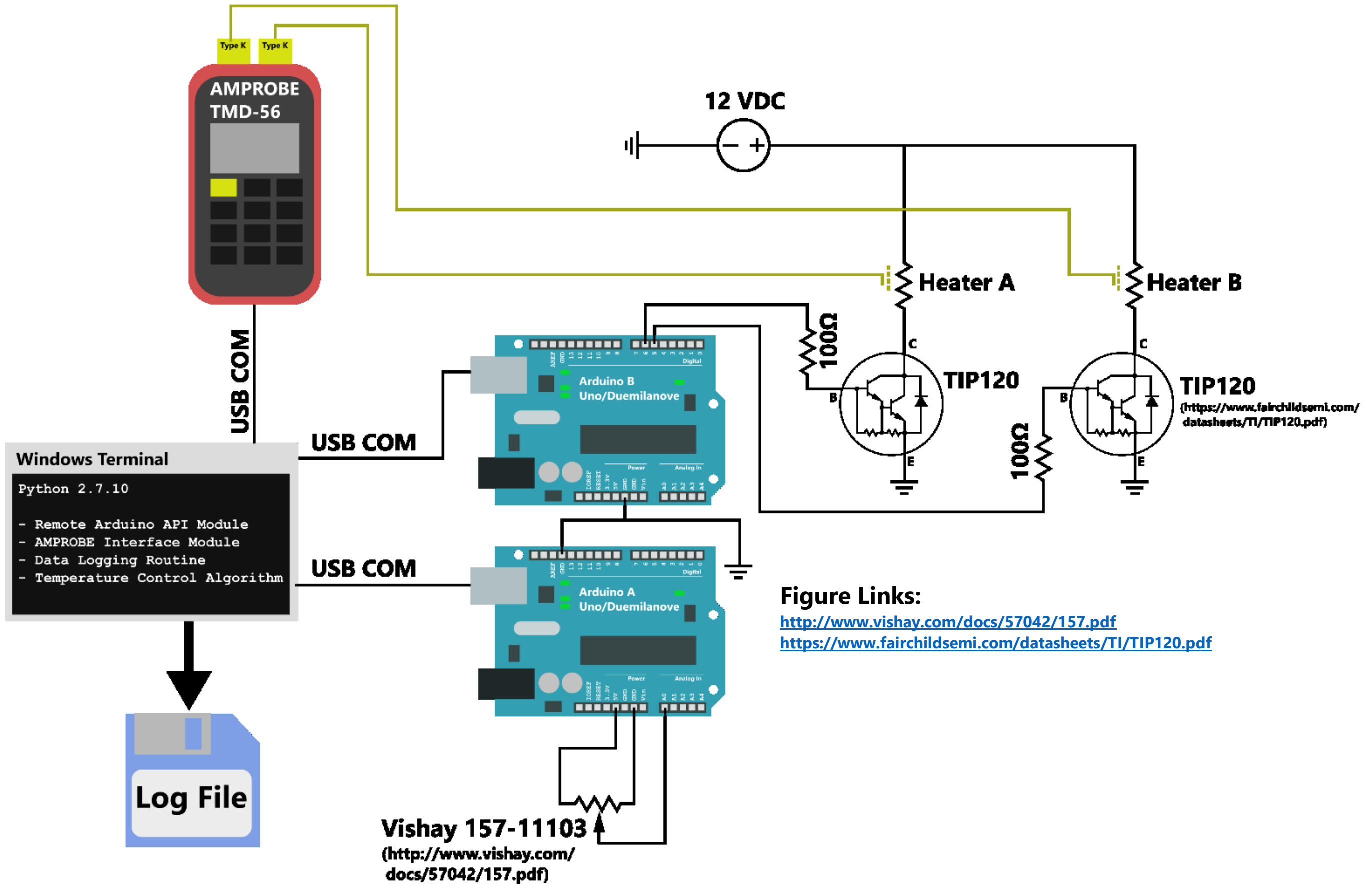

```
Windows Terminal
Python 2.7.10

- Remote Arduino API Module
- AMPROBE Interface Module
- Data Logging Routine
- Temperature Control Algorithm
```

Type K
Type K
AMPROBE TMD-56
USB COM
USB COM
USB COM
Log File
12 VDC
Heater A
Heater B
100Ω
100Ω
TIP120
TIP120
(https://www.fairchildsemi.com/datasheets/TI/TIP120.pdf)
C
B
E
Arduino B Uno/Duemilanove
Arduino A Uno/Duemilanove
Vishay 157-11103
(http://www.vishay.com/docs/57042/157.pdf)
Figure Links:
http://www.vishay.com/docs/57042/157.pdf
https://www.fairchildsemi.com/datasheets/TI/TIP120.pdf

Fig. 10: Antagonistic Fixture Connection Diagram

[3] https://github.com/artisan-roaster-scope/artisan

The schematic for the fixture, including the USB command and file logging architecture, is shown in Fig. 10. Note that the Arduino board was not powerful enough to drive the muscle heater. Instead, each channel was connected to a TIP120 Darlington transistor pair, capable of driving up to 5 A on each channel (for more information, see the datasheet link in Fig. 10). The 12 V power supply was a surplus power brick rated at only 3.35 A, so the TIP 120 was more than sufficient to switch the heater power. The driver circuitry of Fig. 10 was assembled on a solderless breadboard, with alligator clip leads for connecting the driver circuit to the muscle heater assembly.

The test fixture software package comprised the aforementioned modified Arduino Prototyping API, the interpreter program for the AMPROBE thermocouple meter adapted from the *Artisan* project, and a control script called *tempTest.py*. The source code files for the modified libraries and the control script can be found in Appendix B. Note that additional simple scripts were also created, using the same libraries, to facilitate tests without temperature stimuli, and calibration runs. These scripts are omitted from this report for brevity.

For instructions on the configuration and use of the fixture, see Appendix C.

3.4 Rotary Fixture Characterization

The characterizations of Section 3.2 suggested a potential constitutive model for the muscle fibers, but did not present a large amount of data for analysis. To create time-domain datasets suitable for in-silico parameter matching, a series of temperature stimuli were applied to a muscle in the antagonistic configuration.

To ensure that a useful model of the antagonistic fixture could be developed for parameter matching, it was necessary to sample the response of the antagonistic fixture to a known stimulus. A reference extension spring was procured for this purpose. The spring was suspended from a pin and a weight was applied to the spring. A photograph of the spring was captured next to a scale 2 inches in length. The weight applied to the reference spring was changed, and an additional photograph was captured. This procedure was repeated for several different weights.

In an image editing program (GIMP[4]), the lengths of the reference spring and reference length under various loads were approximated graphically. The measurement was made between the centers of the circular hooks at each end of the spring; the resulting pixel lengths were then converted to millimeters by referencing the known length of the scale in the photographs. Finally the spring lengths measured in the sample images were converted to lengths reflecting the distance between the centers of the fixture pins, by adding the difference in the measured inner diameter of the spring loop and the measured outer diameter of the fixture pin. This length data, along with the known load weight data, was used to generate a plot of the reference spring's load response. A linear region of this response curve was selected and subjected to regression; the result was a linear mathematical model for a certain region of the reference spring's operation. Note that the reference spring was assumed to be massless and lossless.

[4] https://www.gimp.org/

The reference spring was attached to the test fixture as shown in Fig. 11. A test weight was applied and the rotor was manually cycled between its endstops for calibration. Finally, the rotor was held manually at the zero position and released, provoking a damped oscillatory response. This process was repeated until five valid sample sequences were collected. The five sample sequences from the reference spring oscillation test were later used in a parameter matching exercise to determine antagonist fixture parameters such as rotational inertia and frictional damping rate.

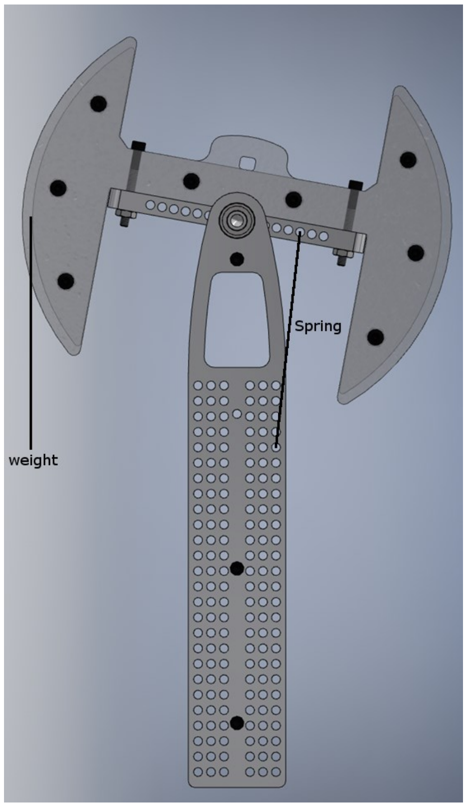

Fig. 11: Spring Test Configuration

Muscle response curves were collected on the rotary fixture by stringing a single two-ply muscle to the fixture, in a manner similar to the spring configuration shown in Fig. 11. No spring was connected to the fixture, but a weight was applied as in the reference spring oscillation test. Initially, the weight was a minimal training mass to provoke the muscle to become taut.

Using the tubular heater described in Section 3.3, the muscle was repeatedly cycled to approximately 90°C and then returned to room temperature. Rotor movement was monitored during this stimulus. Once a roughly repeatable motion was achieved, the cyclic stimulus was terminated and a larger load weight was applied to the fixture. The muscle temperature was stepped incrementally (in a staircase pattern) and returned to room temperature. This temperature sweeping was reiterated until a roughly repeatable motion was achieved. Then, the minimal training mass was applied and the muscle was again cycled between approximately 90°C and room temperature. This process was repeated for various load weights, with temperature cycling at the low training mass between each load weight staircase stimulus.

One final data sequence was produced using a different stimulus function. The muscle was reset using the same low training mass and temperature cycling regime used in the staircase stimulus test. Then, at a test load, the muscle was heated quickly to approximately 90°C and allowed to cool to room temperature. This heating cycle was reiterated, producing a rough sawtooth temperature waveform, until roughly repeatable actuation was observed. Then, at room temperature, the load mass was increased by pouring a known mass of ball-bearings into the load vessel, *without* stopping the test or repeating the training mass cycling regime. The sawtooth heating and cooling cycle was then repeated until roughly repeatable actuation was observed. Additional mass was added once more, and the cycle was repeated. The resulting single output dataset from this test provided a convenient characterization of muscle behavior under changing load.

3.5 Parametric Modeling

To develop a mathematical model for the artificial muscles, it was necessary to manually investigate the results of the preliminary and rotary fixture tests for qualitative behaviors, then characterize these behaviors' relationships with temperature and with each other. Each behavior was separated into a mechanical constitutive linear element (e.g. source, capacitor, dashpot, mass) to simplify the analysis. The constitutive models for each of these effects were assumed to be linear, though the effect of temperature on each effect was not always assumed linear. The conclusions of this process are documented as results in Section 4.2.

In addition to the muscle itself, it was also necessary to develop a simple mathematical model of the rotary antagonistic text fixture. This model assumed simple Newtonian rigid-body response characteristics, with Coulomb friction in the rotating joint.

After the mathematical model was ready, and the model parameters governing the behavior of the muscle and joint fixture models were named, the models were imported to Mathworks Simulink technical simulation software. A few simplifying assumptions were taken during this process; these assumptions are documented in Section 4.2. Note that, at this point, most of the model parameters (except physical constants such as gravitational accelerations) were filled with dummy values.

To determine the muscle-independent parameters of the fixture model, such as damping and rotational inertia, the reference spring model developed in Section 3.4 was imported into Simulink and "installed" in the fixture according to the dimensional structure shown in Fig. 11. The data from the reference spring oscillation tests of Section 3.4 were imported into the modeling environment, and the Simulink Parameter Estimation tool was executed to match the response of the simulated fixture to that of the experimental fixture, under reference spring stimulus. The Parameter Estimation dialog was permitted to vary the damping coefficient and the rotational inertia estimate; this yielded a close-fitting match between the simulation and the five real-life test reference spring oscillation test cases.

To determine the muscle parameters, the reference spring model was removed from the simulation, and the muscle model was "installed" in the fixture according to the dimensional structure used during rotary muscle testing. The data from the staircase muscle tests of Section 3.4 were then imported into the modeling environment, and the Simulink Parameter Estimation tool was executed to match the response of the simulated muscle to that of the experimental muscle. This step was computationally intensive, and therefore proceeded slowly. At some stages, manual adjustments were made in some parameters based on qualitative knowledge of the model not available to the parametric search algorithm. More details on this process and its findings are documented in Section 4.2.

3.6 Controls for Antagonistic Configuration

With a muscle model established, the Simulink test configuration was reorganized to support two simultaneously simulated muscles acting antagonistically. A simple joule heating model for these muscles was adopted, and its heating and cooling rates were set based on an ad-hoc empirical measurement of the fixture's heating and cooling rates.

The heater stimulus channels in the simulated two-channel joint setup were connected to a virtual discrete PID (proportional-integral-derivative) controller. Various steps were taken in an attempt to linearize the system for controls tuning; these steps and their outcomes are documented in Section 4.4. Finally, a controlled system was produced in-silico (i.e. numerical simulation), and the response of the system to various inputs and forcing stimuli were recorded.

4 Results

4.1 Preliminary Test Findings

Preliminary tests comprised mostly ad-hoc procedures on temporary fixtures, plus the detailed characterizations T1 and T2.

The earliest tests did not produce much useful quantitative information. The preliminary testing process demonstrated empirically that the selected precursor (20-lb Trilene XL Smooth Casting nylon fishing fiber) could be coiled into muscle form under a tension of 2.7 N, or 275 grams-force. This value was selected as the standard coiling load for all subsequent testing.

The earliest preliminary tests also revealed several meaningful qualitative muscle properties, which influenced the design of the detailed tests T1 and T2. The muscles tended to permanently increase in length when heated under high load, but they returned to their original length if heated under low load. Furthermore, the muscles exhibited temperature-dependent contraction at all loads, and the degree of contraction (in percentage-points) did not appear to depend on load.

Based on these findings, the procedures for T1 and T2 were developed to characterize the repeatable contraction and non-repeatable deformation behaviors of the muscle fibers, respectively.

T1 yielded data along the axes of temperature, strain, load, and training temperature. Consider first several plots of strain data with respect to load at different peak training temperatures, shown in Fig. 12. In these illustrations, the temperature of each reading is indicated by coloring.

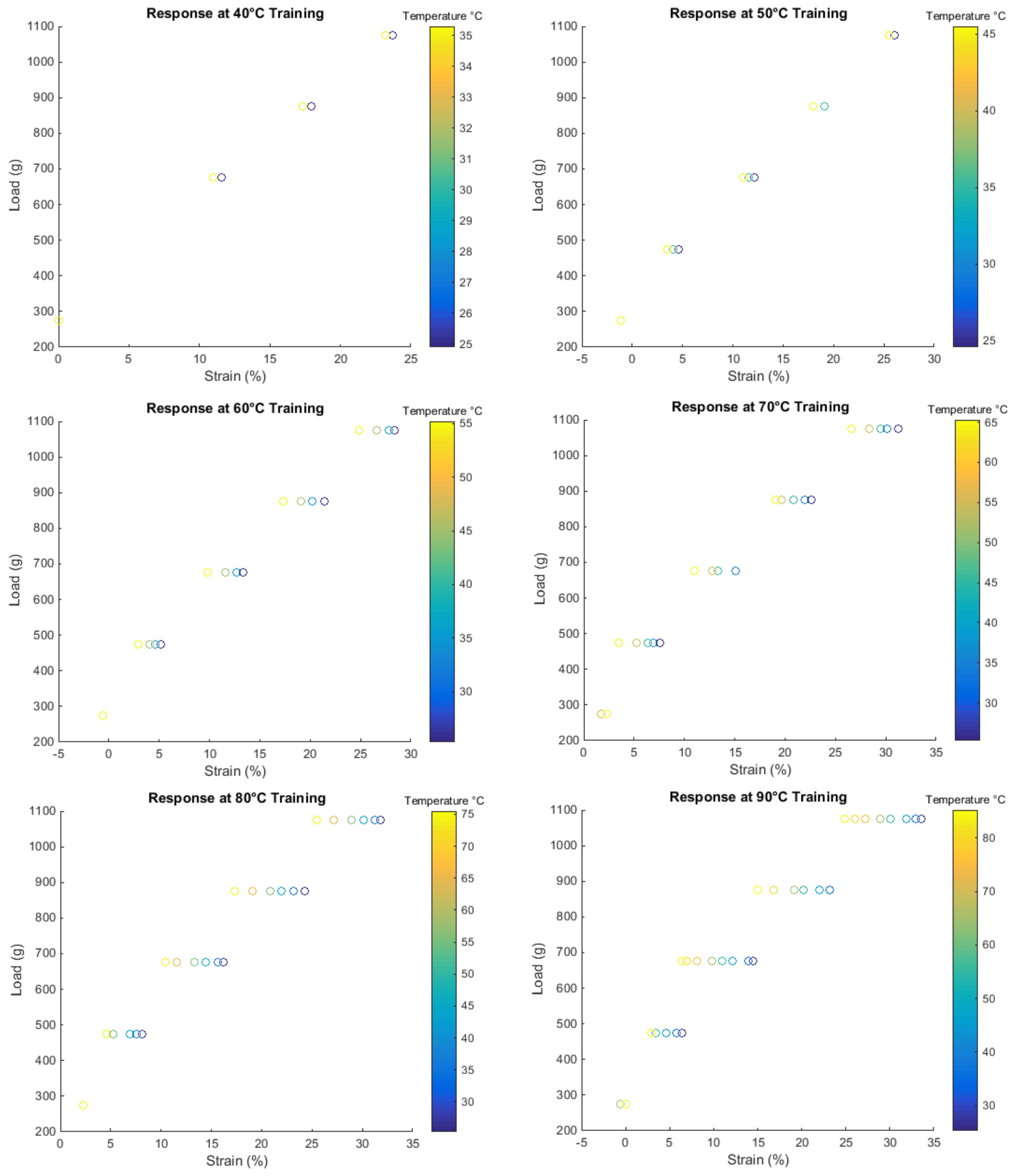

Fig. 12: T1 Raw Response Plots

Note that each of the plots in Fig. 12 describes a consistent contraction during heating, up to an approximately constant strain limit, at which the muscle cannot get any shorter. It appears that this contraction’s absolute magnitude is associated with the temperature, independent of the load on the muscle.

To test this hypothesis, it is possible to strip the resting room temperature positional bias from each horizontal row of data points in the raw plots of Fig. 12. This is achieved by subtracting the strain value of the rightmost point (room temperature) in a given constant-load dataset from each data value within the same dataset. The result is a zero-bias metric indicating the degree of muscle contraction with respect to room temperature strain, herein named the *contraction offset*. Note that this quantity represents *percentage points* of difference in strain, and not percent change relative to any position.

The plot of Fig. 13 illustrates the relationship between the contraction offset and temperature, for all the relevant data points in T1. Each colored line represents a set of data points taken under a fixed load (horizontal tuples in the raw response plots of Fig. 12). Note the boundary condition associated with low loads, which causes a set of lines that stray from the primary trend.

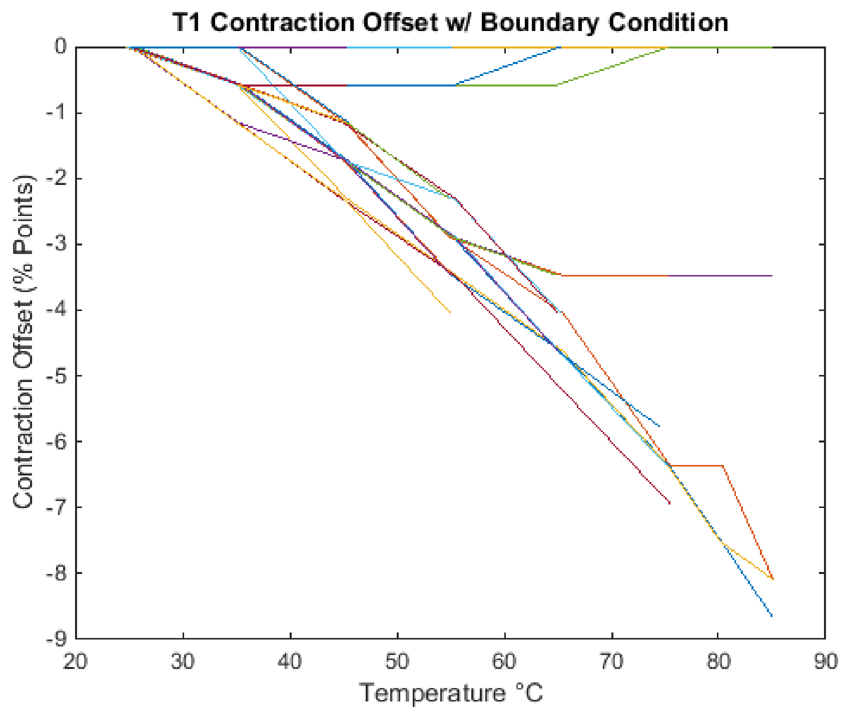

Fig. 13: T1 Contraction Offset for All Samples

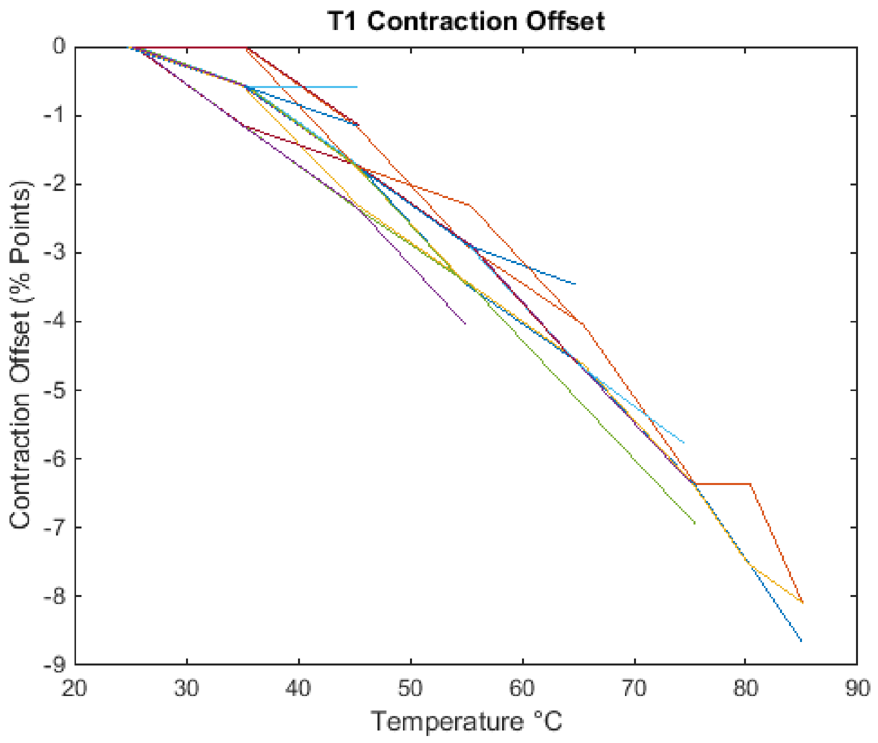

Fig. 14: T1 Contraction Offset w/ Boundary Excluded

The plot in Fig. 14 shows the contraction data for all samples from the previous set of plots, excluding samples taken at 275 g and 475 g loads. It appears that eliminating this region of the sample space also eliminates the boundary effect shown in Fig. 13. Quadratic regression over the resulting dataset produces the fit of equation (3).

$$offset = -0.001279548572343t^2 + 0.001385427266603t + 0.846078596331288 \qquad \textbf{(3)}$$

This fit is shown in Fig. 15.

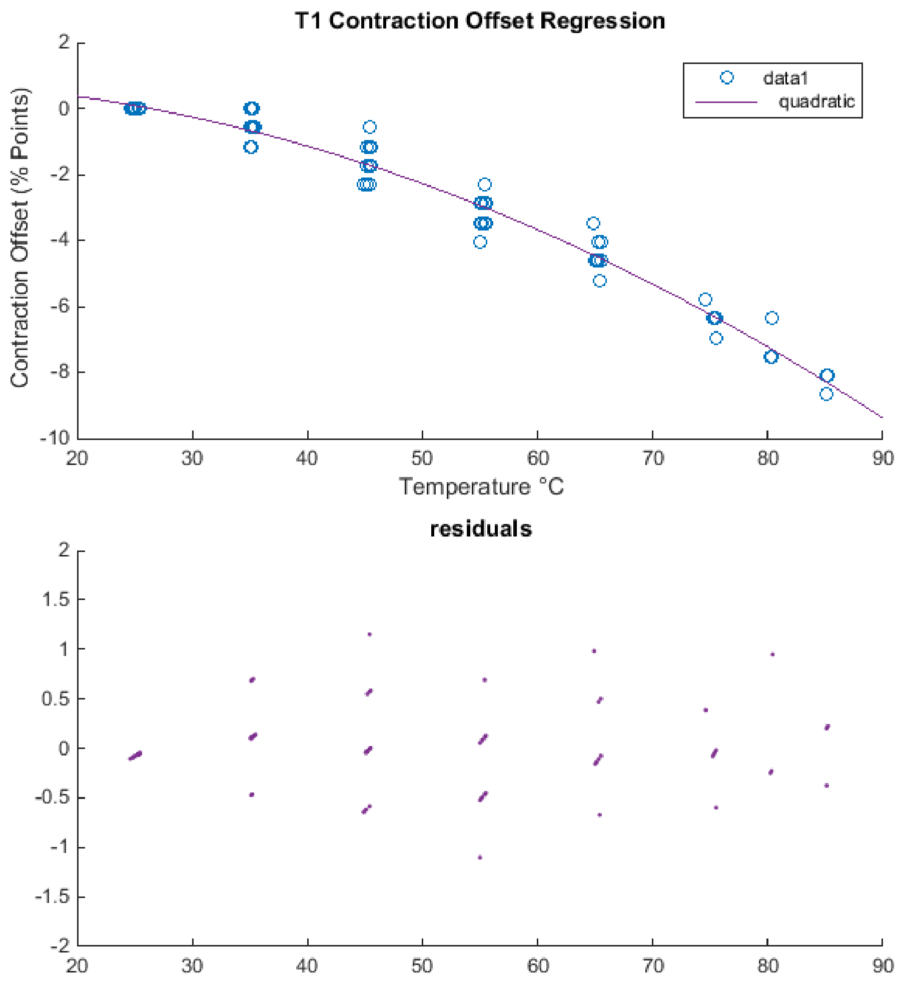

Fig. 15: T1 Contraction Offset Regression

As shown in Fig. 13, a boundary condition prevents the muscle from contracting fully in certain circumstances. In particular, this boundary condition appears to occur when contracting would cause the muscle's overall strain to become smaller than a certain value. The final plot in Fig. 12 shows that this effect is not simply a "hard cutoff"; instead, the contraction offset function changes when the muscle is operating below a strain value of 5%.

The goal of detail testing is to suggest a mathematical model of muscle behavior. To keep this model simple, further analysis will assume low strain conditions (<5%) can be avoided during use, by mechanically forcing the muscle under that minimum tensile strain at all times. With this assumption, and with the newly created regression from Fig. 15, a temporary descriptive model can be created. This model is shown in equation (4).

$$c = -0.00128t^2 + 0.00139t + 0.846$$

$$\sigma = \begin{cases} s + c, & s + c > 5 \\ undef, & s + c < 5 \end{cases} \tag{4}$$

In this model, σ is the actual strain in percentage points, c is the contraction offset computed in Fig. 15, and s is a quantity named "resting length" which must account for all phenomena not attributed to thermal muscle actuation. Future linear tests over artificial muscles must resolve the value of s, resting length, in various operating conditions. Any data point that is collected will be useful in this pursuit, because values for s can be obtained by solving the equation $\sigma = s + c$.

Note that more information can be gleaned from T1, now that a basic model has been established. In particular, T1 shows the value of s when a muscle is subjected to a fixed load and taken to a fixed temperature several times, for a variety of loads and temperatures, when starting from a known state similar to the state of a "virgin" muscle (trained at a high temperature and a low load). By solving the equation $\sigma = s + c$, values of s can be determined in these conditions.

Fig. 16 shows a plot of the values of *s* given by T1 data for several different initial heating temperatures and loads investigated during T1. These values are computed from all valid data points and not just room temperature cases; this is the reason for the vertical lines at each tested load (each line illustrates the range of values observed).

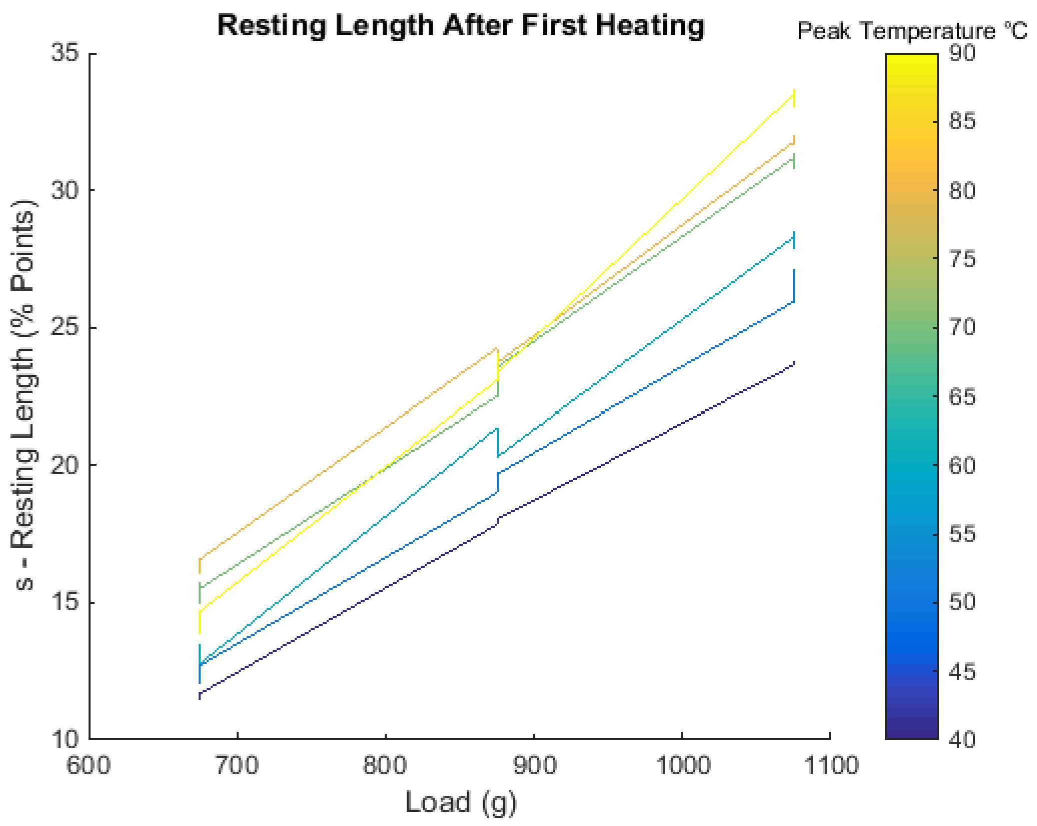

Fig. 16: T1 Values of Resting Length s for Various Loads and Initial Training Temperatures

Fig. 16 reveals that increasing the training load can cause an increase in the resting length, but increasing the peak training temperature does not necessarily increase resting length. It also shows that, near high peak training temperatures, the rate of increase of *s* with respect to the load goes up (in other words, the slope of the *s*-load curve increases).

Regression over this plot is omitted from this report, because the data points are too localized to produce useful regression information. Notwithstanding this fact, Fig. 16 illustrates a strong and conclusive limitation of the polymer artificial muscle technology: *the resting length of the muscle depends strongly upon the current and past values of load and operating temperature,* and this resting length value contributes as much to the overall length of the muscle fiber as the repeatable contraction effect highlighted by Haines *et al.* [5] and documented in Fig. 15.

The behavior of the muscle during thermal cycling was not fully captured during this test; there was not sufficient time to parse and analyze all of these data points. To ensure a proper survey of performance, a sampling of thermal cycling data was selected for parsing, namely the pulsed temperature runs before the 675 g and 1075 g load tests at 90°C, 70°C, and 50°C. Fig. 17 shows all of these selected cycling processes in a single plot. Note that the common "sequence number" axis in Fig. 17 serves merely to illustrate the order of events; each separate outlined block of cycling events occurred at a different point in the T1 process.

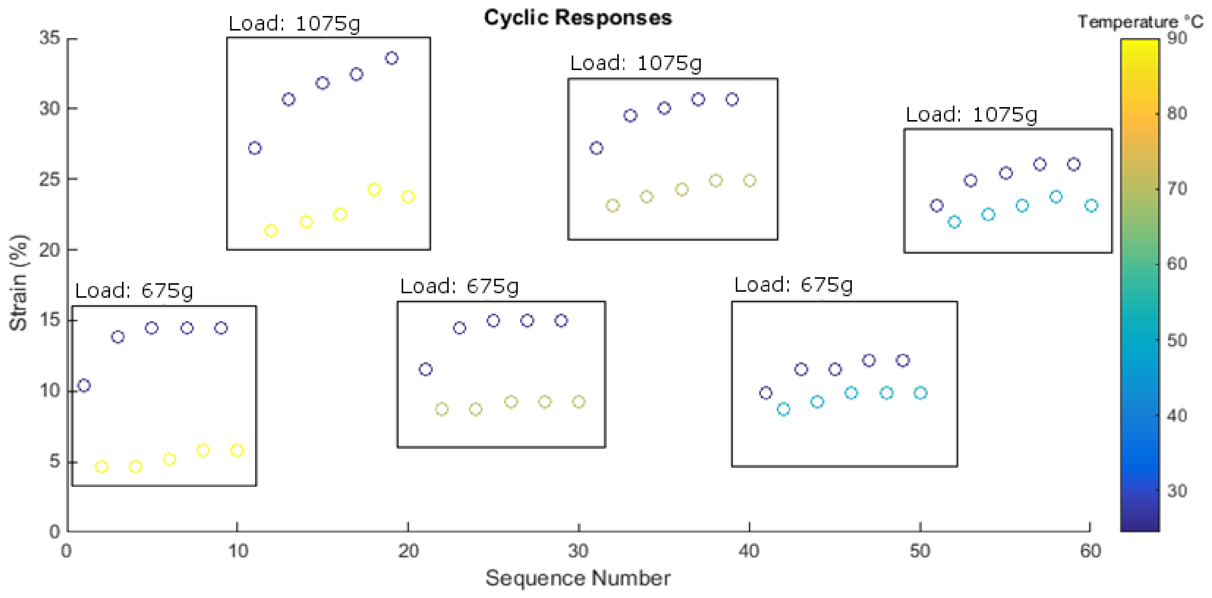

Fig. 17: T1 Cycling Behavior in Select Cases

In each outlined block within Fig. 17, the first sample occurs at room temperature, and the muscle is repeatedly heated to a higher temperature. Fig. 17 illustrates that the first heat cycle has the greatest effect on muscle resting length. At low loads or temperatures, this first heat cycle appears to completely “train” the muscle to its new resting length. At higher loads and temperatures, specifically the instance in which the 1075 g load is applied and the muscle is cycled to 90°C, the muscle resting length keeps increasing slightly with each cyclic application of heat. In other words, the result in Fig. 17 shows that thermal cycling has a much stronger effect on training during the first training cycle than on subsequent cycles. Only at high loads and temperatures does a significant cyclic non-repeatability become evident.

Note that, to reduce time requirements, thermal cycling beyond the first training cycle was not performed during T2, based on the conclusions from the data shown in Fig. 17.

Test T2 attempted to address a high-dimensional field of data, namely the hysteretic response of the resting muscle length s, using a reasonably small number of test data points. Unfortunately time did not permit a sufficiently complex analysis of the sample space of possible muscle temperature histories. Proper evaluation of muscle hysteresis in a reasonable timeframe would require the use of an automatic thermomechanical analyzer, which was not available for this test. Such an investigation may also require interpretation of high-dimensional data, a complex mathematical problem which falls outside the scope of this project. Because of these shortcomings, the results of T2 have been determined to be irrelevant for characterizing muscle response, and are omitted here.

4.2 Model Findings

The selected model structure for the rotary fixture (independent of the muscle model) is shown in Fig. 18.

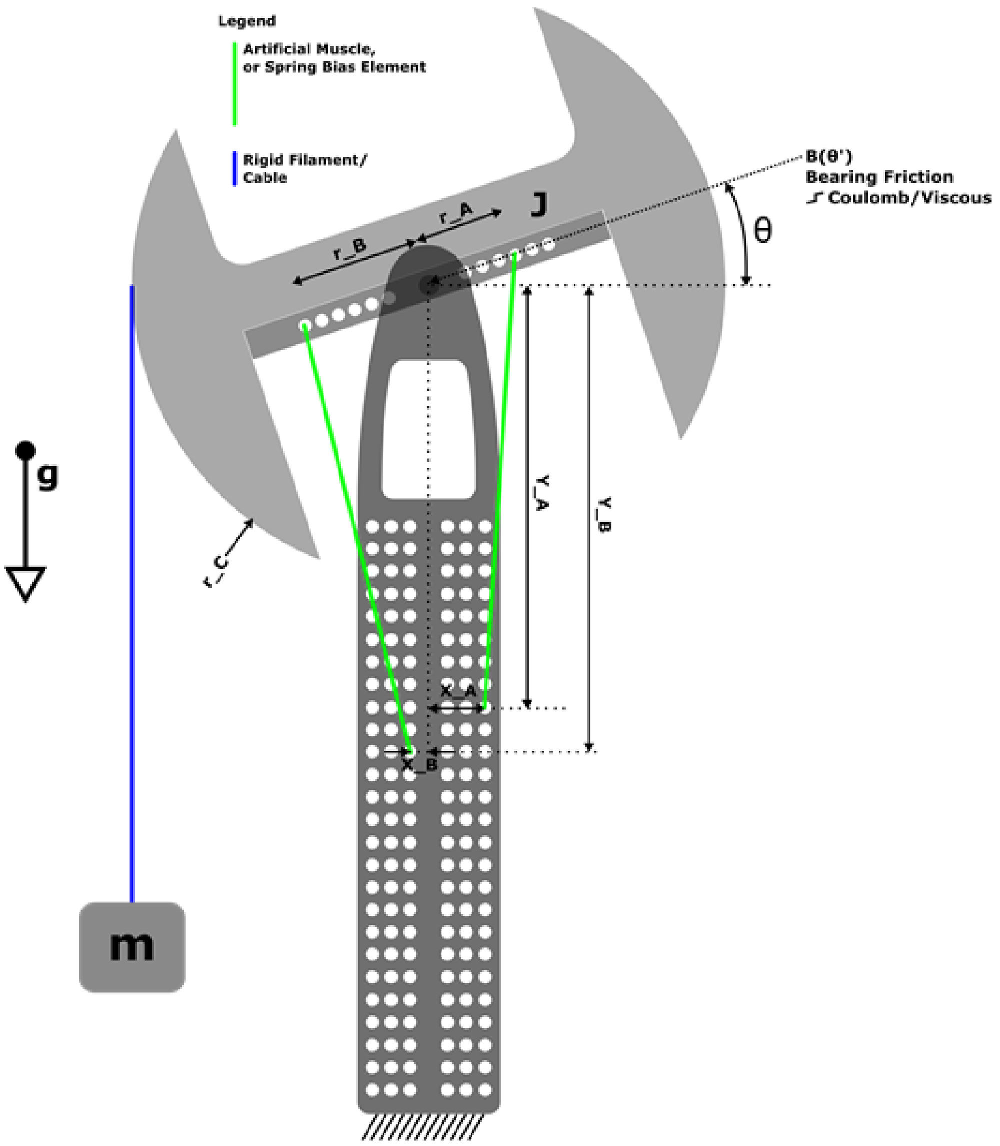

Fig. 18: Antagonistic Test Fixture Equivalent Model (adapted from [28])

The system of Fig. 18 is a simple dynamical rotor, without plane motion. The simple differential equation representation for this rotor is omitted here, as it is easily input directly to Simulink using symbolic elements. Note that the friction in the rotor is not assumed to be a linear velocity damper, and is instead modeled more accurately using an assumed Coulomb friction function.

The complicating factors in this model are the non-linear modulated transformer functions between the muscle/spring stimulus elements and the rotor. These elements possess length and tension properties, which impose torque functions on the rotor. To compute these torque functions, vector mathematics must be applied. The known vectors are:

$$\vec{A} = \hat{\imath}X_A - \hat{\jmath}Y_A$$

$$\vec{B} = -\hat{\imath}X_B - \hat{\jmath}Y_B$$

$$\overrightarrow{r_A} = \hat{\imath}r_A\cos\theta + \hat{\jmath}r_A\sin\theta$$

$$\overrightarrow{r_B} = -\hat{\imath}r_B\cos\theta - \hat{\jmath}r_B\sin\theta$$

The vectors of interest, namely the muscle/spring elements, can now be defined in terms of known quantities. The conclusive vectors are shown in equations (5) and (6); the vector lengths are shown in equations (7) and (8).

$$\overrightarrow{M_A} = \vec{A} - \overrightarrow{r_A}$$

$$\overrightarrow{M_B} = \vec{B} - \overrightarrow{r_B}$$

$$\overrightarrow{M_A} = -\hat{\imath}r_A\cos\theta - \hat{\jmath}r_A\sin\theta + \hat{\imath}X_A - \hat{\jmath}Y_A \quad \textbf{(5)}$$

$$\overrightarrow{M_B} = \hat{\imath}r_B\cos\theta + \hat{\jmath}r_B\sin\theta - \hat{\imath}X_B - \hat{\jmath}Y_B \quad \textbf{(6)}$$

$$L_A = \left|\overrightarrow{M_A}\right| = \sqrt{(X_A - r_A\cos\theta)^2 + (-Y_A - r_A\sin\theta)^2} \quad \textbf{(7)}$$

$$L_B = \left|\overrightarrow{M_B}\right| = \sqrt{(-X_B + r_B\cos\theta)^2 + (-Y_B + r_B\sin\theta)^2} \quad \textbf{(8)}$$

The length of each muscle/spring is now known in terms of the angle θ of the rotor. The torque on the rotor due to each muscle/spring element is a function of both rotor position (the modulating factor) and the tensile force in the muscle/spring element, named $F_{A/B}$ here. The conclusive torque quantities are shown as equations (9) and (10).

$$\overrightarrow{\tau_A} = \overrightarrow{r_A} \times \overrightarrow{F_A} = \begin{vmatrix} \hat{\imath} & \hat{\jmath} & \hat{k} \\ r_A \cos\theta & r_A \sin\theta & 0 \\ \frac{F_A}{L_A}(X_A - r_A\cos\theta) & \frac{F_A}{L_A}(-Y_A - r_A\sin\theta) & 0 \end{vmatrix}$$

$$= \hat{k}\left(\frac{F_A r_A}{L_A}\cos\theta\,(-Y_A - r_A\sin\theta) - \frac{F_A r_A}{L_A}\sin\theta\,(X_A - r_A\cos\theta)\right) \qquad \textbf{(9)}$$

$$\overrightarrow{\tau_B} = \overrightarrow{r_B} \times \overrightarrow{F_B} = \begin{vmatrix} \hat{\imath} & \hat{\jmath} & \hat{k} \\ -r_B \cos\theta & -r_B \sin\theta & 0 \\ \frac{F_B}{L_B}(-X_B + r_B\cos\theta) & \frac{F_B}{L_B}(-Y_B + r_B\sin\theta) & 0 \end{vmatrix}$$

$$= \hat{k}\left(-\frac{F_B r_B}{L_B}\cos\theta\,(-Y_B + r_B\sin\theta) + \frac{F_B r_B}{L_B}\sin\theta\,(-X_B + r_B\cos\theta)\right) \qquad \textbf{(10)}$$

While both of these expressions are non-linear, they are easily computed by simulation software and will therefore permit accurate simulation of fixture response without assumptions about the position of the rotor. Note that the lengths of the muscle/spring elements have also been computed; these serve as inputs to the constitutive models for the muscles and reference spring within the simulation. Those constitutive models produce force outputs, which may in turn be used to compute the torques on the rotor using equations (9) and (10).

Note that the rotary antagonistic fixture was not capable of simultaneously heating an entire muscle to a consistent temperature; a length of the muscle under test was always resting at room temperature outside of the heating tube. To account for this effect without increasing model complexity, the “effective temperature” of the muscle in the simulated model was defined using a weighted average, as in equation (11):

$$T_{eff} = \frac{L_{heater}T_{heater} + (L_{muscle} - L_{heater})T_{room}}{L_{muscle}} \tag{11}$$

The model for the reference spring was determined empirically and takes the form shown in equation (12), where F is the tensile force in the spring in Newtons, and x is the length of the spring in meters, measured between the two mounting pins on the antagonistic test fixture.

$$F = 145.71x - 5.2097, \qquad x \geq 0.04682 \tag{12}$$

This linear model depicts a lossless capacitive element, which in turn is a good representation for an extension spring that is not in saturation.

The constitutive model for the muscle itself was the most complicated aspect of the modeling exercise in this project. Based on the results from Section 4.1, a muscle model structure had to account for the following observed effects:

1) MODULUS: The muscle exhibits a spring-like behavior, wherein any applied force generates a proportional deformation strain.
2) HYST: The muscle exhibits a temperature- and load-history-dependent training effect, wherein the muscle's "resting length" can be modified by manipulation of temperature and load.
3) OFFSET: The muscle is prone to contraction when subjected to a temperature increase. The magnitude of the contraction in terms of absolute distance (percentage *points* strain) is a strong function of temperature, and does not depend on muscle load, if the other two observed effects are ignored. In this sense, the contraction appears in same ways analogous to the manipulation of the position input of a common series-elastic actuator.

The MODULUS effect is the easiest to model; it is merely a linear spring. The OFFSET effect is also simple to model, because this effect appears to occur independent of the other system effects. Thus the OFFSET can be modeled as a true positional offset source, with offset magnitude a function of temperature, positioned in series with the MODULUS element.

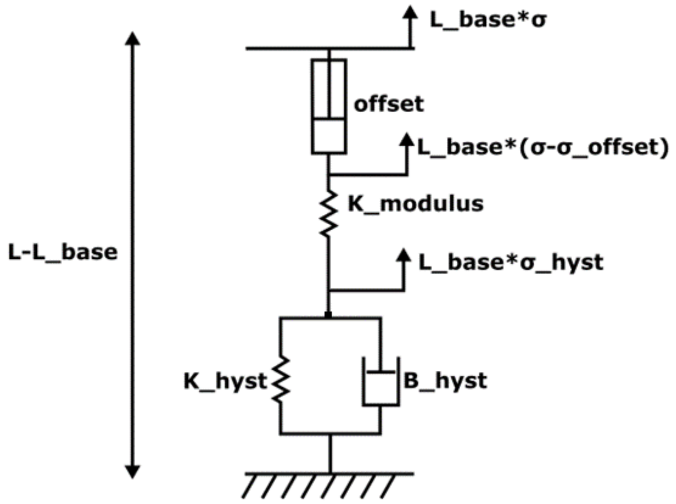

Fig. 19: Muscle Model

The HYST effect is the most difficult to model, but it is common to use damper models for hysteretic effects. In fact, researchers working with polymer artificial muscles coiled from conductive thread showed that a damper model accurately described isothermal load-cycling hysteresis within their muscles (an effect not directly investigated here) [21]. A model based on this work provides a convenient starting point for this case. A fixed damper model in parallel with a spring models isothermal hysteresis, but more detail must be added to account for the muscle's memory of its resting length. If a damper's coefficient is negatively dependent upon temperature, the damper will permit fast deformations at high temperatures, but resist them at low temperatures, preventing recovery from a deformation achieved at high temperature. This is an accurate description of the observed muscle behavior. Thus, the HYST effect is modeled using a linear spring and damper in parallel, with the damper's coefficient dependent upon temperature. For simplicity, the temperature dependence of the damper element is assumed linear.

The model as described above is illustrated in Fig. 19. Note that this model does not account for the mass of the muscle, which is assumed to be negligible relative to the masses in the antagonistic rotary test fixture.

From this point in the analysis, it is convenient to assess response in terms of relative strain. This strain will be assessed with respect to a "base length", refined as the minimum length of the muscle before it has deformed. Strain is denoted in the simulation work associated with this paper using the character *sigma* (σ); this notation is continued here.

$$\sigma = \frac{L - L_{base}}{L_{base}}$$

And so:

$$L = L_{base} + \sigma L_{base}$$

The most convenient mathematical interpretation of the muscle model will take L or σ as an input, and produce the resulting tensile force as an output. Certain simplifications are necessary to accomplish this inversion. First, the springs must be modeled as tensile springs, which can only produce tensile force, and which cannot actuate below a certain threshold force. To invert this region of saturation, it is necessary to introduce a slight incline to the otherwise sharp cliff of saturation. Thus, a very small strain value ϵ is selected, and the spring forces follow in equations (13) and (14):

$$F_{K_{hyst}} = \begin{cases} L_{base}(\sigma_{hyst} - \epsilon)K_{hyst} + F_{hyst_{min}}, & \sigma_{hyst} > \epsilon \\ \frac{F_{hyst_{min}}}{\epsilon}\sigma_{hyst}, & 0 < \sigma_{hyst} \le \epsilon \\ 0, & \sigma_{hyst} \le 0 \end{cases} \tag{13}$$

$$F_{K_{modulus}} = \begin{cases} L_{base}(\sigma - \sigma_{offset} - \sigma_{hyst} - \epsilon)K_{modulus} + F_{modulus_{min}}, & \sigma - \sigma_{offset} - \sigma_{hyst} > \epsilon \\ \frac{F_{modulus_{min}}}{\epsilon}(\sigma - \sigma_{offset} - \sigma_{hyst}), & 0 < (\sigma - \sigma_{offset} - \sigma_{hyst}) \leq \epsilon \\ 0, & (\sigma - \sigma_{offset} - \sigma_{hyst}) \leq 0 \end{cases} \tag{14}$$

In equations (13) and (14), the expressions $F_{hyst_{min}}$ and $F_{modulus_{min}}$ are the minimum forces required to begin deforming the respective springs. The expression for damping is simple:

$$F_{B_{hyst}} = B_{hyst}L_{base}\dot{\sigma_{hyst}}$$

The sum of the forces is computed as follows, and yields a final differential equation representation in equation (15).

$$F_{B_{hyst}} + F_{K_{hyst}} - F_{K_{modulus}} = 0$$

$$B_{hyst}L_{base}\dot{\sigma_{hyst}} = F_{K_{modulus}} - F_{K_{hyst}}$$

$$\dot{\sigma_{hyst}} = \frac{F_{K_{modulus}} - F_{K_{hyst}}}{B_{hyst}L_{base}} \tag{15}$$

The value of σ_{offset} must be defined. The results from Section 4.1 showed that the offset element obeys a temperature law, which has been measured empirically. A quadratic relation appeared to provide a suitable temperature law, so the offset function is defined accordingly in equation (16):

$$\sigma_{offset} = AT^2 + BT + C \tag{16}$$

Note that, for consistency with the rest of the model, the value of σ_{offset} was defined to have units of *pure fractional strain*, not percentage points. This is a departure from the notation used in Fig. 15 and related tests.

Finally, the relation between temperature and the coefficient of the HYST damping element must be defined. A linear relation is selected for simplicity, as shown in equation (17):

$$B_{hyst} = H_{B_{hyst}} \left(T + T_{hyst_{offset}} \right) \tag{17}$$

All of the models documented here were simple enough to ingress into the MATLAB/Simulink environment. The Simulink model subsystem for the muscle itself is shown in Fig. 20. The complete subsystem for the fixture, configured with a single muscle, is shown in Fig. 21. Finally, the test configuration for the entire system (set up for the sawtooth test stimulus) is shown in Fig. 22.

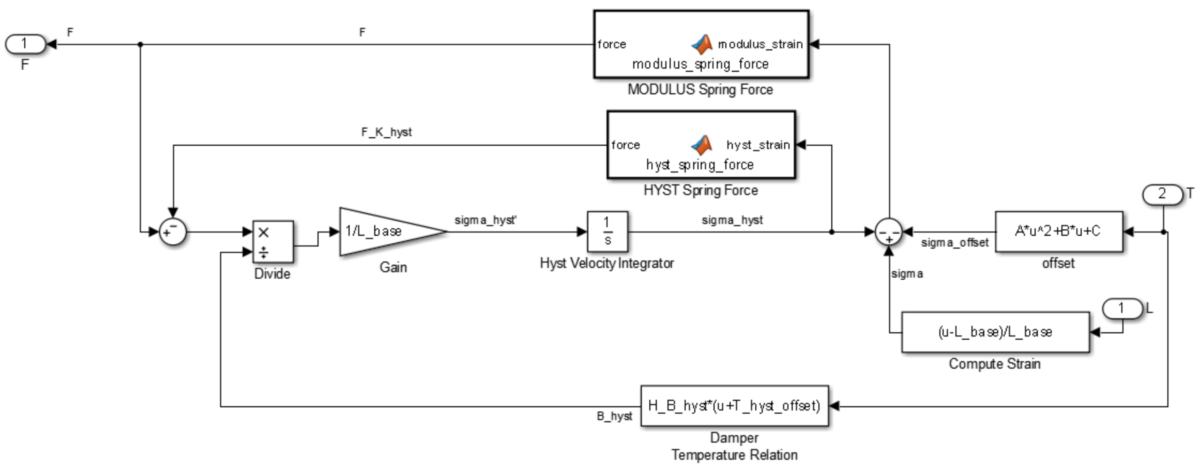

Fig. 20: Simulink Muscle Subsystem

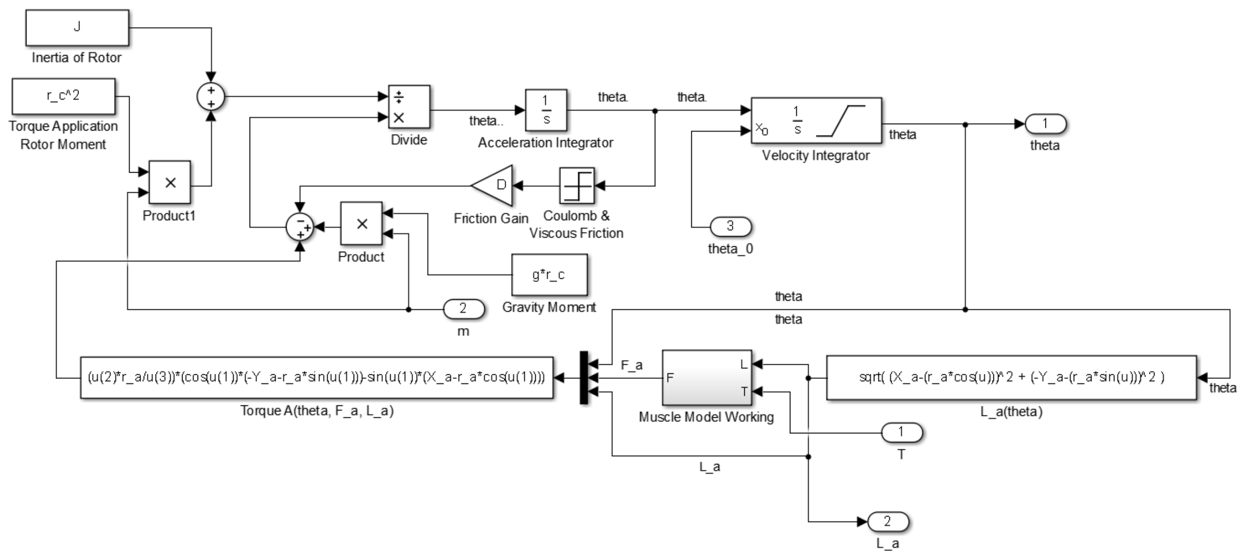

Fig. 21: Simulink Joint Subsystem w/ One Muscle

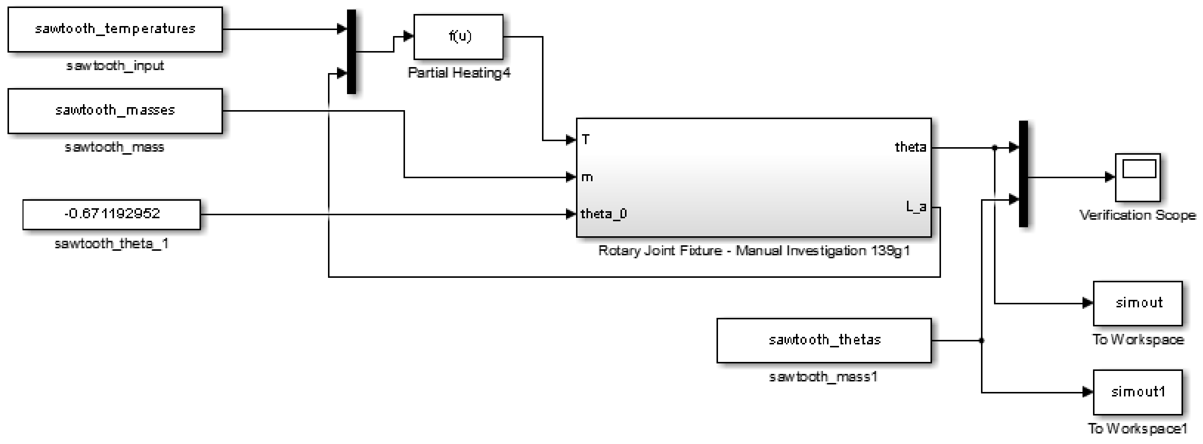

Fig. 22: Complete Simulink Model w/ Experimental Stimulus

4.3 PARAMETER ESTIMATION FINDINGS

Before the parameters of the muscle could be determined, it was necessary to find the values of the rotor rotational inertia and damping. This was accomplished using the Simulink Parameter Estimation utility, over the five reference spring oscillation sample sets collected before muscle testing. Two separate parameter estimations were performed, one using the more accurate Coulomb damping model, and another using the less accurate but simpler linear damping model.

Table 1 shows the results of the reference spring parameter matching exercise.

Table 1: Reference Spring Oscillation Parameter Matching Results

Test Configuration	Parameter	Value
Coulomb Damping	Inertia J	$0.00124103\ \mathrm{kg-m^2}$
	Damping D	$0.00545940\ \mathrm{N-m}$
Linear Damping	Inertia J	$0.00131390\ \mathrm{kg-m^2}$
	Damping D	$0.00415667\ \mathrm{N-m}$

The reference spring parameter matching exercise was trivial due to the small number of parameters under investigation. The muscle parameter matching exercise was much more computationally intensive and therefore slower. The parameters under analysis were $\left[F_{hyst_{min}}, K_{hyst}, F_{modulus_{min}}, K_{modulus}, H_{B_{hyst}}, T_{hyst_{offset}}, A, B, C\right]$. The $F_{modulus_{min}}$ and $K_{modulus}$ parameters could be easily estimated based on the initial resting state of the system, but the remaining parameters had to be estimated computationally. Three staircase stimulus datasets with different load weights were selected as the estimation experiments; the data from these tests were imported into Simulink and a nonlinear parameter estimation exercise was executed (note that the Coulomb damping model was used for the fixture model in this step). The results of the estimation exercise are shown in Table 2.

Table 2: Muscle Model Parameter Estimation Results

Parameter Name	Value	Estimation Technique
A	$-1.17832\mathrm{e}-05\ 1/\mathrm{K}^2$	Computational Search
B	$1.40992\mathrm{e}-05\ 1/\mathrm{K}$	Computational Search
C	0.00881695	Computational Search
$F_{hyst_{min}}$	$1.75489\ \mathrm{N}$	Computational Search
K_{hyst}	$415.189\ \frac{\mathrm{N}}{\mathrm{m}}$	Computational Search
$F_{modulus_{min}}$	$3.789\ \mathrm{N}$	Manual Estimation
$K_{modulus}$	$186\ \frac{\mathrm{N}}{\mathrm{m}}$	Manual Estimation
$H_{B_{hyst}}$	$-545.907\ \frac{\mathrm{N-s}}{\mathrm{m-K}}$	Computational Search

$T_{hyst_{offset}}$	-243.380 ℃	Computational Search

The estimation response curves are shown alongside the experimental data curves in Fig. 23, Fig. 24 and Fig. 25. Note that all the data in these three figures were used as reference data in the parameter estimation exercise.

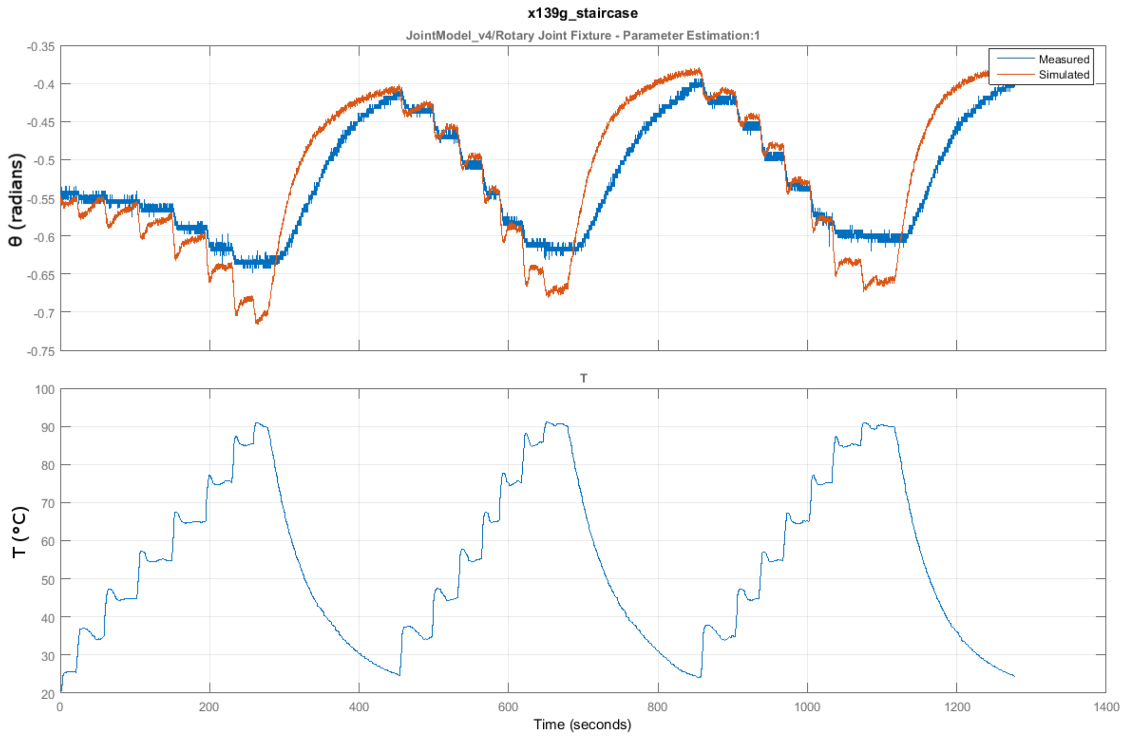

Fig. 23: 139g Stimulus Experiment Parameter Matching Comparison

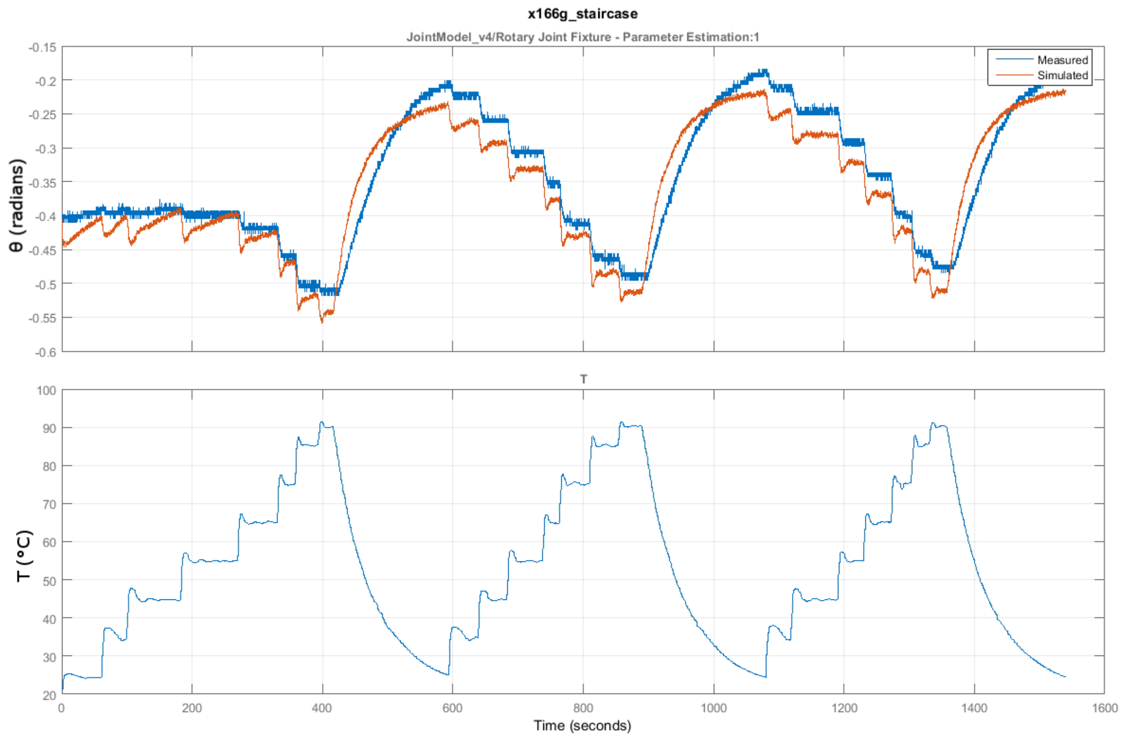

Fig. 24: 166g Stimulus Experiment Parameter Matching Comparison

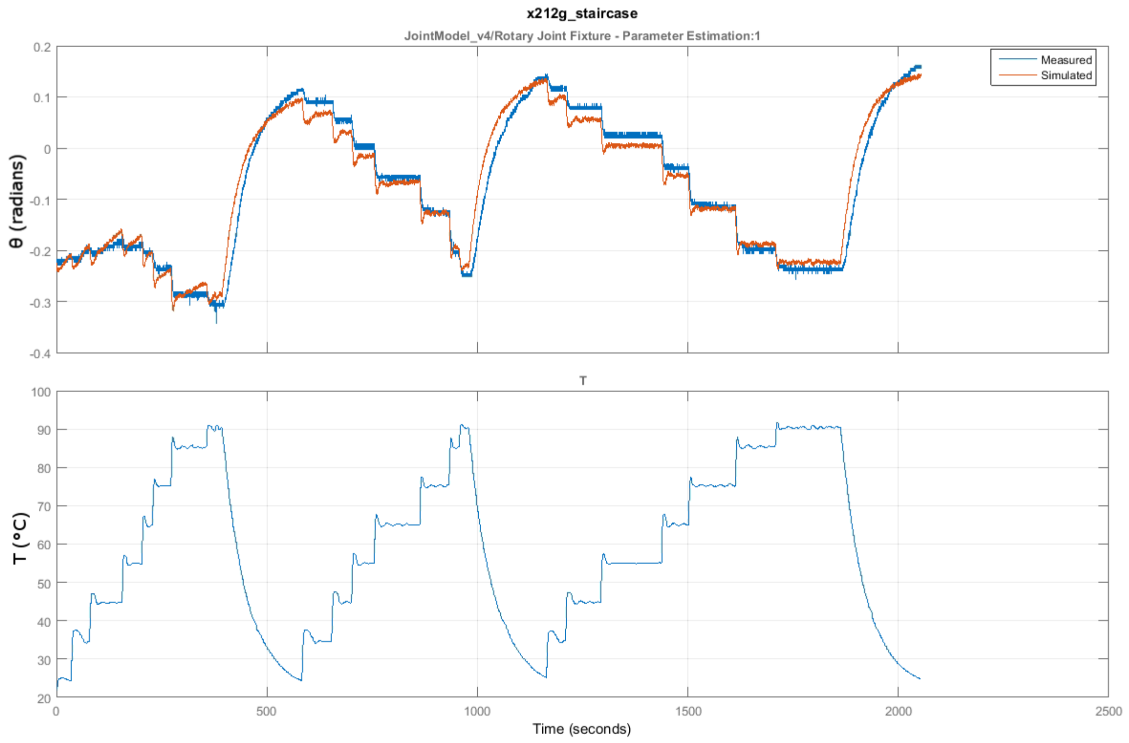

Fig. 25: 212g Stimulus Experiment Parameter Matching Comparison

Because all the staircase datasets were used in parameter estimation, the sawtooth dataset was selected as a downstream verification dataset. The output of the simulated system, when stimulated using the temperature curve from the sawtooth experiment, is shown in Fig. 26.

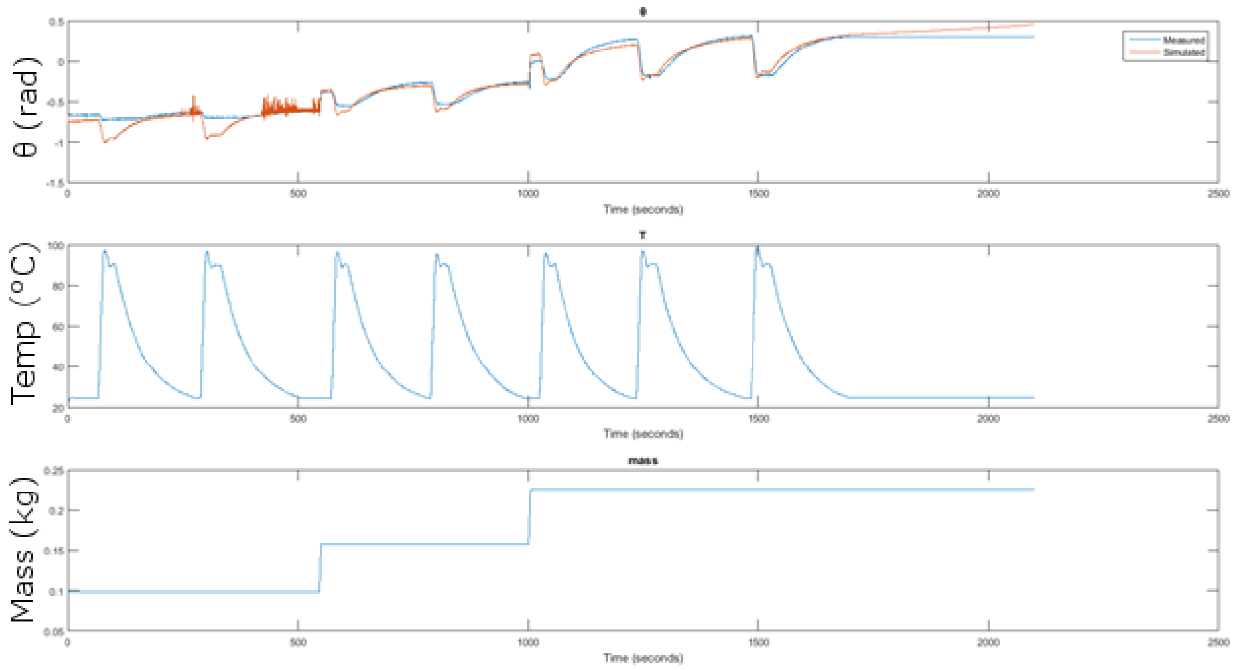

Fig. 26: Downstream Verification Comparison of Measured and Simulated Response Datasets for Sawtooth Stimulus Experiment

Note that the downstream verification plot closely follows the general trend of the experimental plot. The saturation condition (in which the coils of the muscle fiber press up against one another) was not modeled in the simulated muscle element, and the resulting error in response can be observed in the first two peaks of Fig. 26. Simulation noise can also be observed in the first two relaxations of Fig. 26; this noise was caused by overshoot inside the spring saturation regions of the muscle model. If these two phenomena are ignored, the simulated response appears to be an accurate reproduction of the real-world system output.

To confirm the above assumptions about the origins of error in Fig. 26, the muscle model and simulation configuration were augmented using small changes designed to address hypothetical problems. First, a simple model for the saturation condition illustrated by Fig. 26 was introduced to the augmented muscle model. The condition was modeled as a very rigid spring with coefficient K_ϵ, only actuating for $\sigma < 0$, as described by equation (18):

$$F_\epsilon = \begin{cases} K_\epsilon \sigma, & \sigma < 0 \\ 0, & \sigma \geq 0 \end{cases} \tag{18}$$

The force F_ϵ of equation (18) was added to the muscle force, which effectively placed the rigid saturation spring in parallel with the muscle model. Note that the "slack muscle" condition was not modeled; it was assumed that the muscle remained taut during the entire test process. The resulting augmented muscle model is shown in Fig. 27.

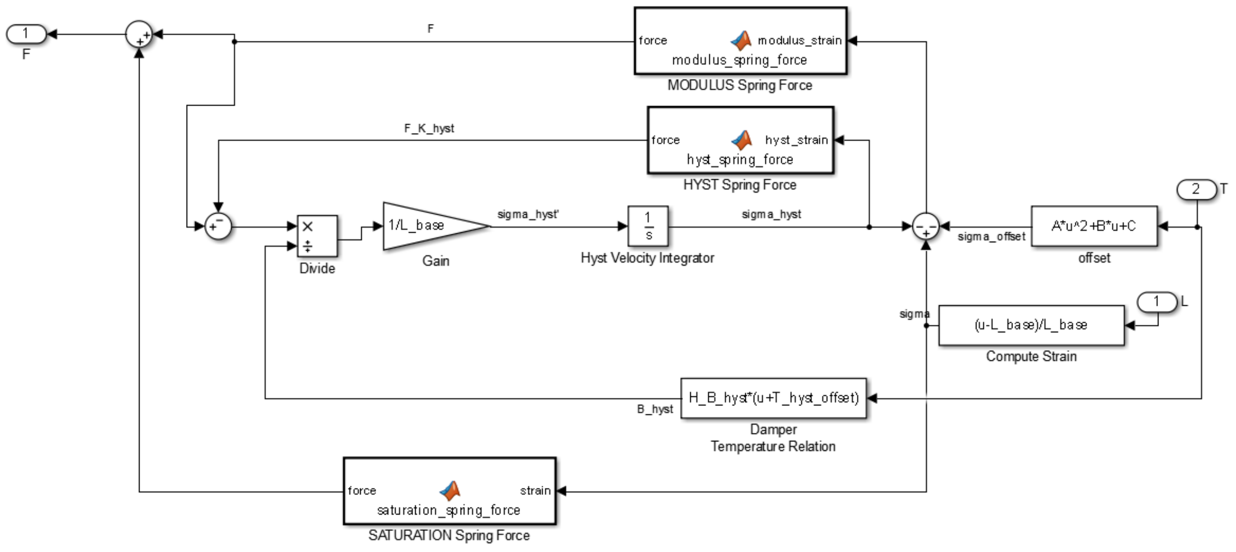

Fig. 27: Muscle Model w/ Added Saturation Condition

After the saturation model was added to the simulation, the time resolution of the simulation was increased, and the parasitic parameters ϵ and K_ϵ were manually adjusted to eliminate the noise effect. The resulting plot, with saturation added and resolution increased, is shown in Fig. 28 (the temperature and mass datasets are omitted, as these plots are identical to those shown in Fig. 26). Fig. 28 confirms that the changes made during augmentation reduced the errors observed in Fig.

26, and further confirms that the augmented muscle model is a close analog for the real-world muscle. Note that while the augmented muscle model is the best model produced thus far, Fig. 28 cannot itself serve as an evaluation metric for the computerized parameter estimation attempt, because the augmented model was influenced by additional human modeling decisions made *in light* of the response to the downstream verification dataset. Fig. 28 simply provides evidence that the hypothesized sources of error in Fig. 26 were in fact true sources of error.

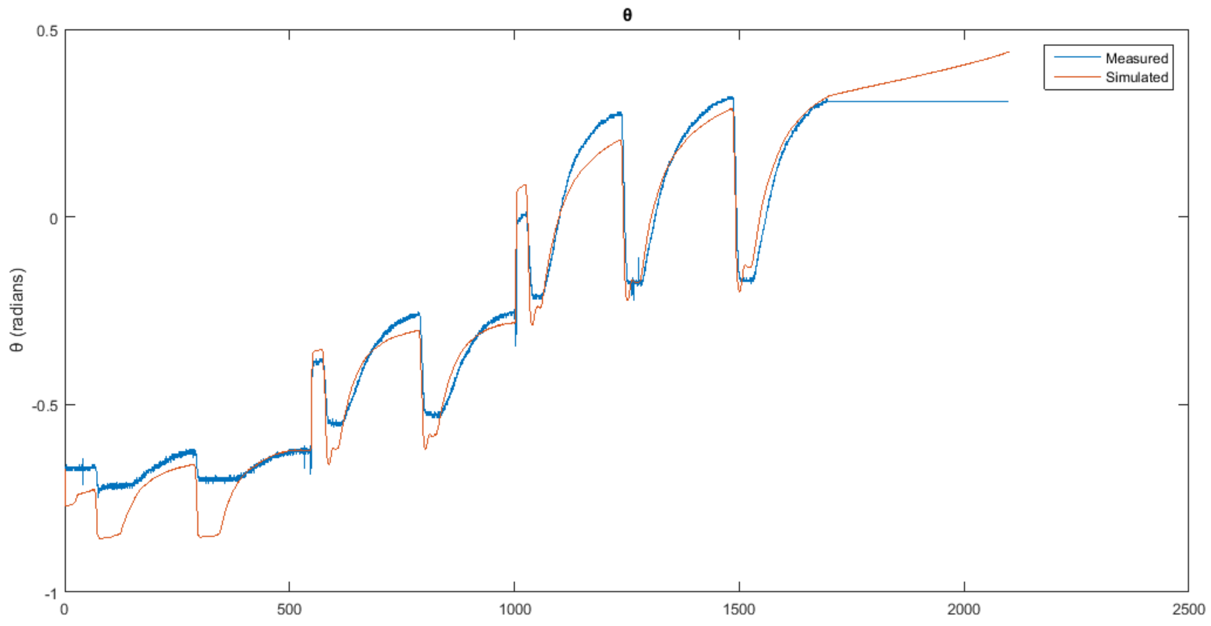

Fig. 28: Augmented Muscle Model Response to Downstream Verification Sawtooth Stimulus

A future version of the model might benefit from a non-linear temperature-damper relation, or even Coulomb-style damping, in the HYST element of the muscle. Such a change could eliminate unwanted drift in the simulated response at room temperature, which can be observed near the end of the time series of Fig. 26 and Fig. 28.

4.4 Controls Findings

The ultimate goal of this project was to develop an environment for investigating controls for polymer artificial muscles, and to demonstrate a potential controls model. For simplicity, PI (proportional-integral) control was selected as the controller type. Simulink conveniently includes a discrete PI controller block, so the test simulation environment was set up around that controller block.

For the in-silico controls test, the simulated joint model was updated to include two antagonistically coupled muscle models, as shown in Fig. 29.

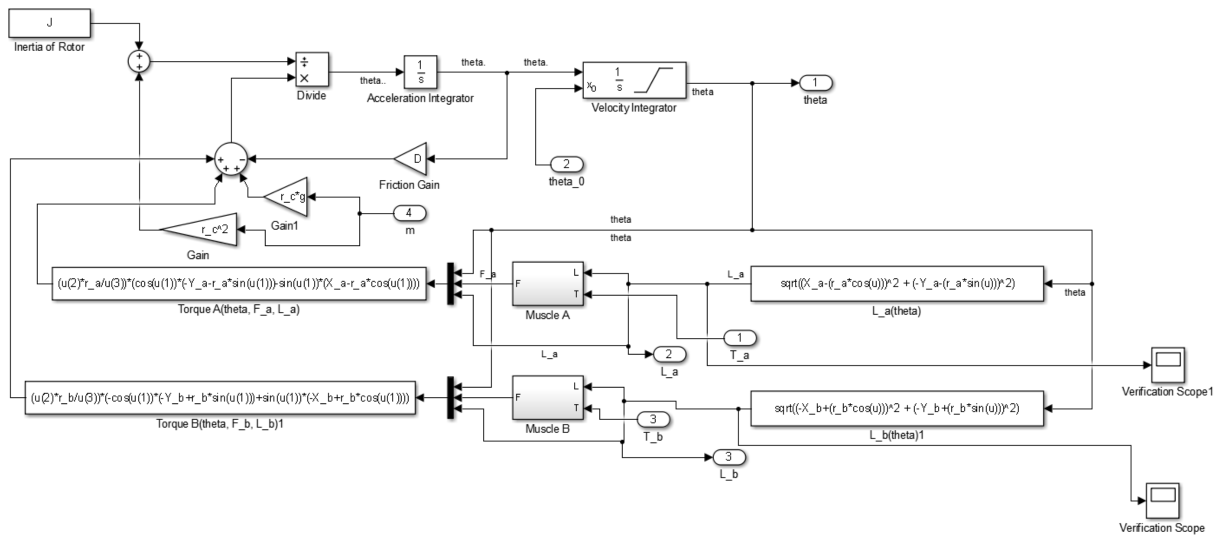
J
Inertia of Rotor
Divide
1/s
Acceleration Integrator
theta..
theta.
theta.
x0 1/s
Velocity Integrator
theta
1 theta
D
Friction Gain
2 theta_0
r_c*g
Gain1
4 m
r_c^2
Gain
theta
theta
(u(2)*r_a/u(3))*(cos(u(1))*(-Y_a-r_a*sin(u(1)))-sin(u(1))*(X_a-r_a*cos(u(1))))
Torque A(theta, F_a, L_a)
F_a
F L T
Muscle A
L_a
sqrt((X_a-(r_a*cos(u)))^2 + (-Y_a-(r_a*sin(u)))^2)
L_a(theta)
theta
1 T_a
L_a
2 L_a
Verification Scope1
(u(2)*r_b/u(3))*(-cos(u(1))*(-Y_b+r_b*sin(u(1)))+sin(u(1))*(-X_b+r_b*cos(u(1))))
Torque B(theta, F_b, L_b)1
F L T
Muscle B
3 T_b
sqrt((-X_b+(r_b*cos(u)))^2 + (-Y_b+(r_b*sin(u)))^2)
L_b(theta)1
3 L_b
Verification Scope

Fig. 29: Antagonistic Simulation Arrangement

Note that this antagonistic model used the simpler, linear model for damping, instead of the non-linear Coulomb model. The antagonistic model also included the augmented version of the muscle model, described in Section 4.3.

Heating was simulated using a linear energy flow model, and cooling was simulated according to Newton's cooling law. The rate coefficients for each of these models were empirically measured using a real heater tube, so the simulated heating and cooling rates would match real-world properties for the antagonistic test fixture. While the real fixture used PWM signals to control heating, the simulated model used a true analog scaling function to emulate PWM. This simplification allowed the model to run at a lower time-precision. The true scale of the Arduino's PWM signal function (0-255) was used as the input scale of the linearized PWM element, to facilitate easy transfer of the model in-silico to a real-world implementation.

The controller output was limited to one muscle at a time: positive controller output stimulated one muscle, while negative controller output stimulated the other. The full controller model, encapsulating the rotary fixture subsystem, is shown in Fig. 30. This figure represents the culmination of work in this project, as no real-world antagonistic controller testing was performed.

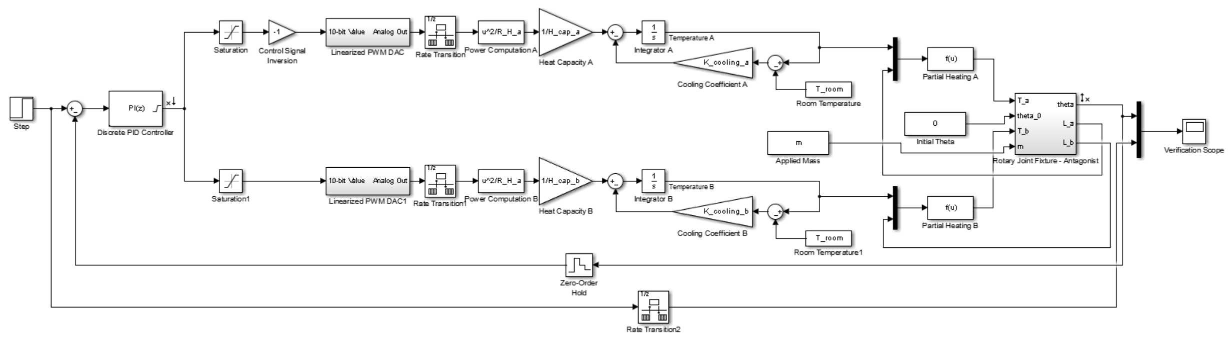

Fig. 30: In-Silico Antagonistic Controller System

The plant of Fig. 30 could not be linearized automatically by the computer, so a closed-loop manual linearization was performed using Simulink's built in PID Tuner Closed Loop Snapshot Linearization tool. Manual best-guess P and I parameters were selected, and the closed-loop snapshot was taken near the end of a step-response plot. Simulink's built-in PID tuner was then allowed to estimate parameters for a high-speed controller. The step response for the computationally-tuned controller is shown in Fig. 31.

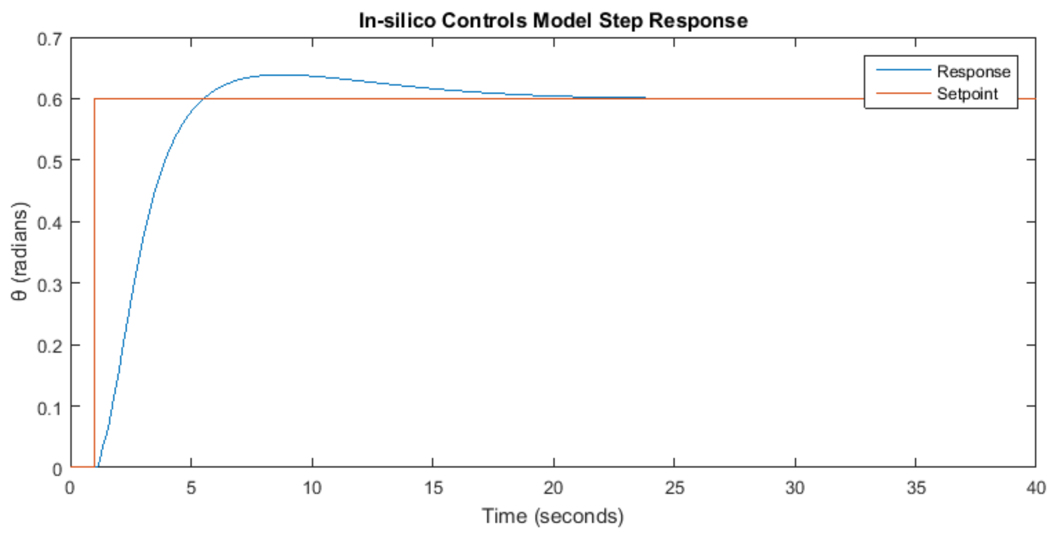

Fig. 31: PI Controller Step Response

The effect of “re-training” in the HYST element of the muscle model provoked concern about the PI controller’s ability to maintain zero steady-state error during repeated cycling events and non-constant loads. To test the validity of this concern, various test stimuli were applied to the in-silico model.

First, a symmetric pulsed input was applied. The response is shown in Fig. 32.

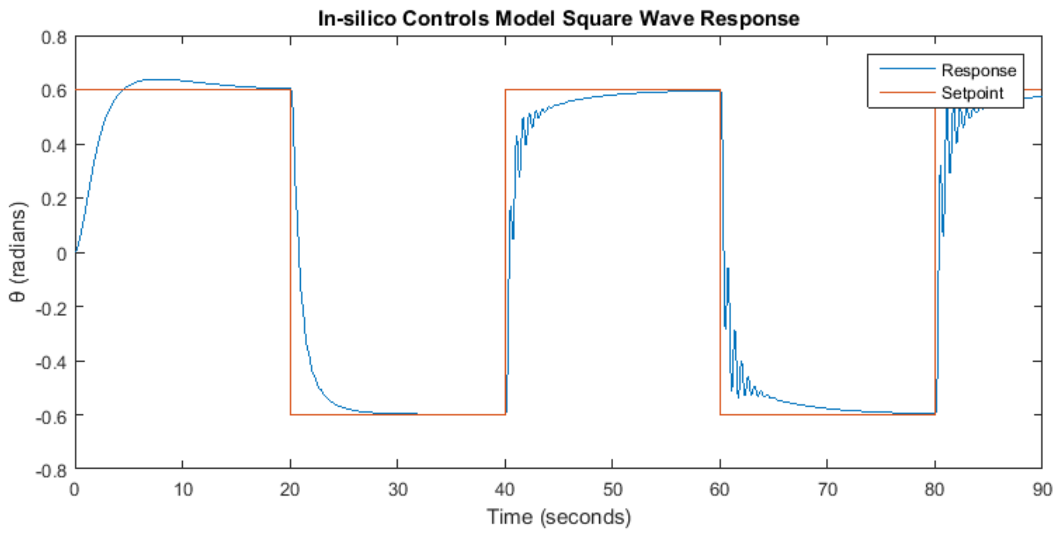

Fig. 32: PI Controller Square Response

Next, a step input was applied, and a mass stimulus was applied instantaneously, after a delay period. The response is shown in Fig. 33. This outcome serves to illustrate the rotary system's ability to compensate for changes in applied load.

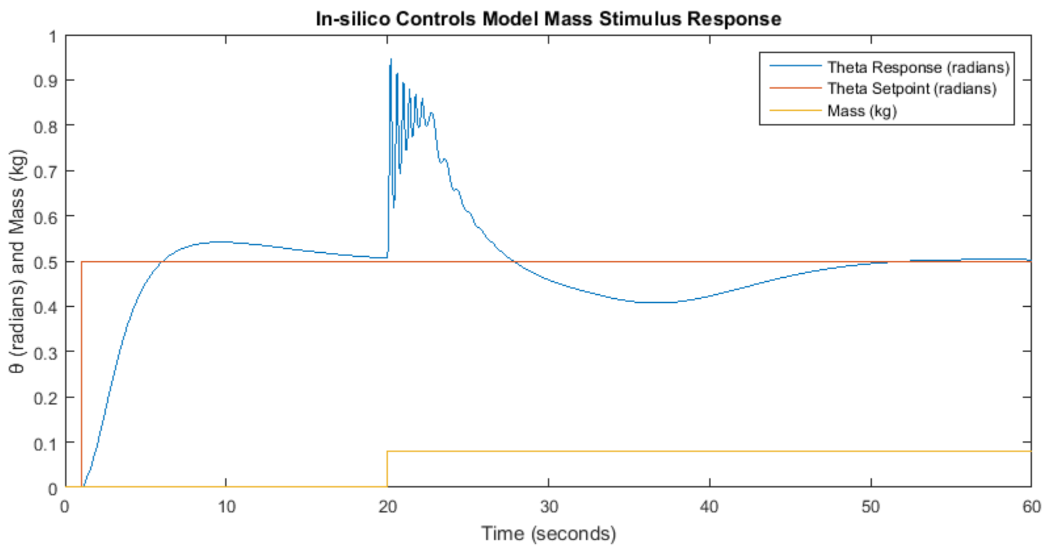

Fig. 33: PI Controller Mass Step Response

Next, during a normal step response, the mass stimulus was fluctuated using sine wave functions of increasing frequencies. The resulting response curves are shown in Fig. 34, Fig. 35 and Fig. 36. Note that the system is highly sensitive to external load stimulus, because of the intrinsic pliability present in the MODULUS element of the muscle model.

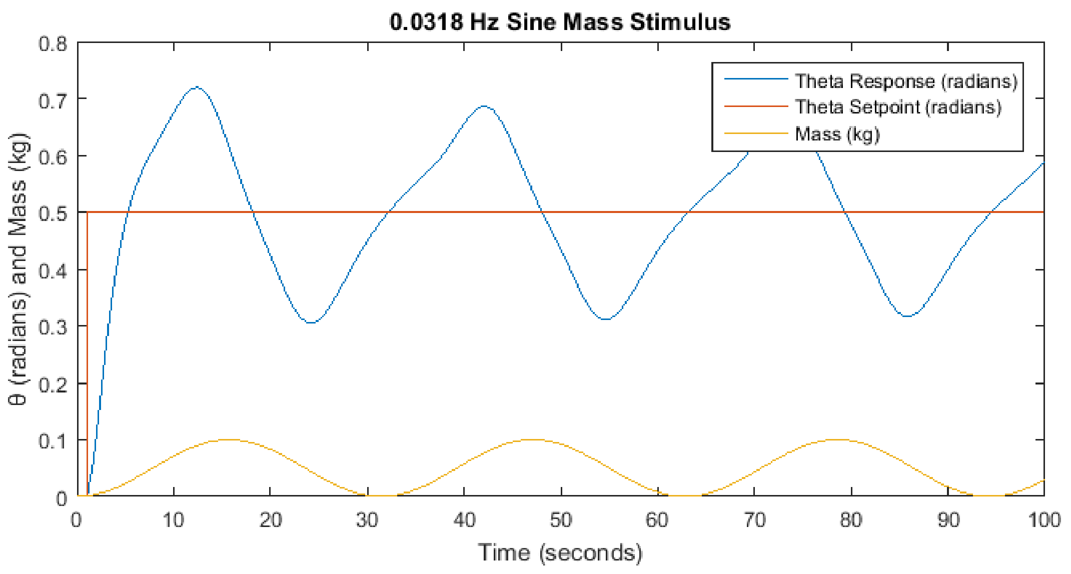

Fig. 34: PI Controller Response to 0.0318 Hz Sine Mass Stimulus

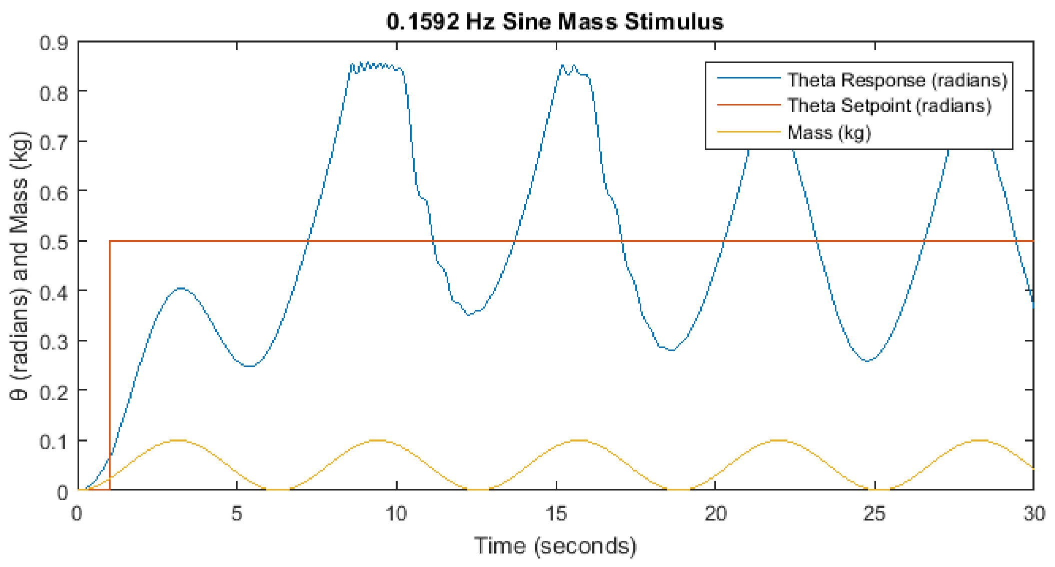

Fig. 35: PI Controller Response to 0.1592 Hz Sine Mass Stimulus

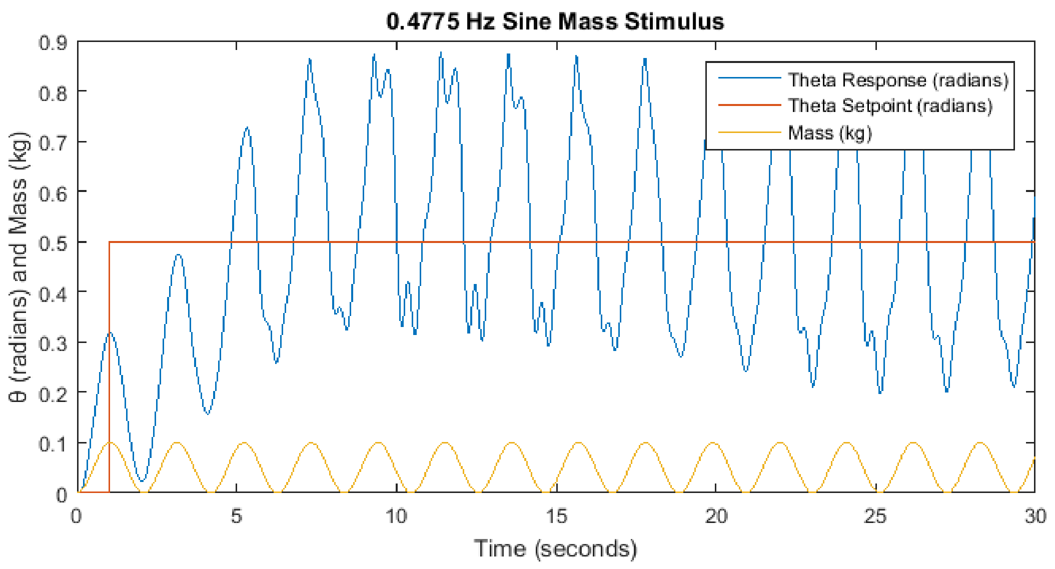

Fig. 36: PI Controller Response to 0.4775 Hz Sine Mass Stimulus

Finally, the mass was set to zero, and the setpoint function was stimulated using sine waves of various frequencies. The resulting response curves are shown in Fig. 37, Fig. 38 and Fig. 39. Note that the system is prone to runaway oscillation if the setpoint changes too rapidly, but that reasonably close tracking is obtained as long as the setpoint stimulus changes slowly.

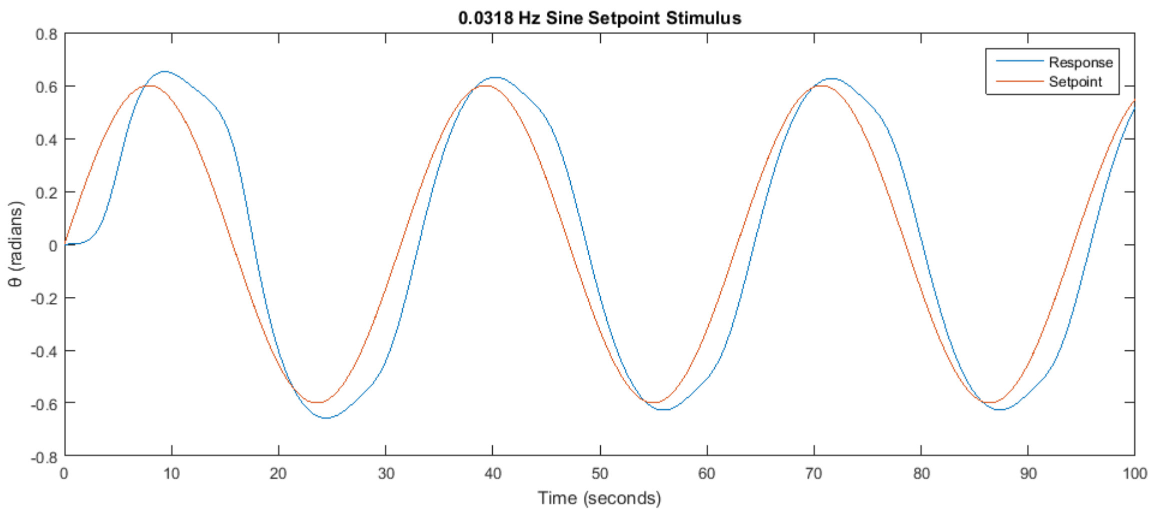

Fig. 37: PI Controller Response to 0.0318 Hz Sine Setpoint Stimulus

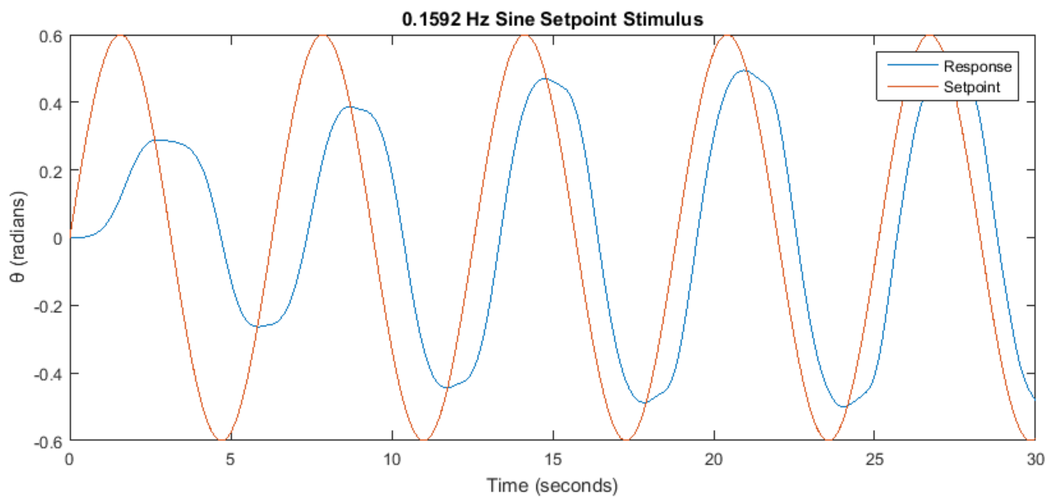

Fig. 38: PI Controller Response to 0.1592 Setpoint Stimulus

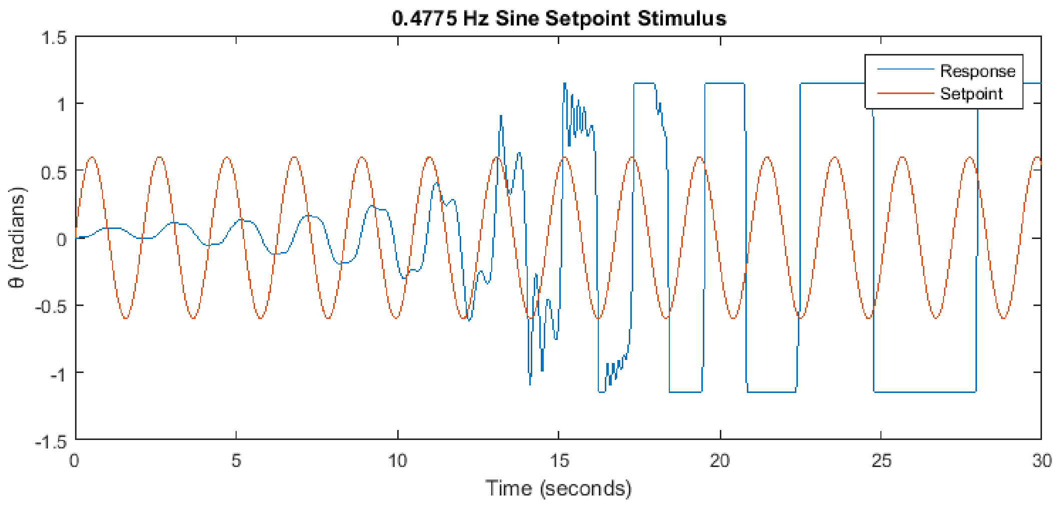

Fig. 39: PI Controller Response to 0.4775 Hz Sine Setpoint Stimulus

5 Discussion and Conclusions

5.1 Application Notes

The international patent application [22] referenced in the seminal work [5] lists several potential applications for the coiled artificial muscles. Proposed applications include pumps and valve drivers for small-scale or even microscopic equipment, spacecraft solar panel expansion/alignment, car door lock actuation (and other solenoid applications), peristaltic pumps using sequentially actuated fiber segments, optical device actuators, haptic feedback devices, porosity control, and various other applications. This section treats a few of those proposed applications in context of the controls findings from the project.

In brief, this project found that twisted polymer artificial muscles could actuate repeatably under constant loads, but changed operating region ("resting length") when subjected to varying loads during operation. This outcome suggests that applications for the muscles fall into two broad categories: those that impart unpredictably varying tension on the fiber element, and those that produce repeatable or constant loading profiles. Instances that require constant loading profiles are immediate candidates for application of the muscle technology discussed herein, as the muscles become very easy to model when they do not undergo a change in resting length. Examples include some valves and pumps, solenoid applications, optical device actuators, and purely visual event controllers (e.g. facial features on a humanoid robot).

Use cases in which the load profile range is unpredictable, or simply very wide, may still be candidates for application of twisted polymer muscle technology, but these applications will require more careful control and may exhibit range-of-motion limitations. Examples of more challenging applications include haptic feedback, complex manifold control and pumping, reversible spacecraft solar panel or solar sail expansion, and pure robotics actuation (e.g. humanoid joint movement). Recent work by Yip and Niemeyer [21] showed that twisted polymer muscles spun from whole conductive threads (rather than monofilaments) made suitable actuators for a robotic hand. That research did not investigate or report on in-situ training effects, which could impact grasping strength or limit muscle range of motion, but the success of a relatively complex application bodes well for this technology.

Note that the applications for twisted polymer muscles are not identical to those applications previously documented for traditional muscle analogs, though there is some overlap. The polymer muscles are especially flexible, and very weight-efficient, so they are well suited to space applications. Because of their low power efficiency, they are poorly suited for traditional power robotics applications such as dynamic manipulation. Nevertheless, as shown in this project, these artificial muscles may still find applications in power robotics. Consider a robotic linkage containing clutches, brakes or dampers at its joints. This kind of element is common if an armature will be subjected to unknown forces, or simply needs to be back drivable. Twisted polymer muscles may satisfactorily control the dynamical parameters in those kinds of auxiliary drive elements, while more traditional actuators execute primary actuation maneuvers.

5.2 FURTHER RESEARCH

Targets for future research include more precise thermal characterizations of muscle properties, better mathematical modeling, mitigation methods for the "retraining" effect, and faster cooling. Specifically, future projects should investigate surface-layer or intrinsic heating elements, rather than using large external heater tubes with unnecessarily high heat capacities. Haines *et al.* [5] and Mirvakili *et al.* [25] have already shown that silver coatings or paints can be used as surface-layer heating elements. Yip and Niemeyer [21] have demonstrated that this method of heating still works when muscles are coiled from whole threads (rather than monofilaments). At a minimum, it is recommended that future experimenters attempt to obtain pre-plated precursor fibers or the proper SPI Flash-Dry paint compound, in order to reproduce the heating elements from [5] and/or [25].

The major challenge for surface-layer heating is cost, as silver is typically the conductive agent. A safe, flexible, low cost alternative surface heating agent would be useful to drive down the cost of high-speed muscles. This is a potential area for future research.

The issue of re-training during loading at temperature remains a controls challenge, though many applications can avoid this problem by imparting predictable loads on the muscle. Yip and Niemeyer [21] did not report the re-training effect, but their muscles were constructed from thread precursors, and treated during "initial training" at a higher peak temperature. It is possible that one of these changes in precursor or process reduced the muscles' propensity for complex hysteretic behavior ([21] reports a fairly straightforward hysteresis loop effect during isothermal load variation). Further investigation or coordination with those researchers may reveal useful information.

The geometric means by which the polymer muscles achieve actuation should be transferrable to other materials with similar molecular structures. Further research into the materials background for the effects documented herein could reveal a precursor material that yields higher efficiency, or reduces the re-training effect.

In a push toward testing efficiency, future projects should work to develop more precise, more automated, non-inertial test fixtures, in which applied force functions are generated using a control system and not using a hanging weight or spring. This development effort could be avoided by the acquisition of a thermomechanical analysis machine, but there will always be some advantages to developing custom test fixtures with the target application in mind.

5.3 Project Conclusion

The research performed in this project demonstrated that the twisted polymer artificial muscles of Haines *et al*. [5] contain useful features, but are also subject to certain mechanical limitations associated with model complexity. While other researchers have characterized the initial training of the muscle, no known published work has documented the property of re-training during load changes at high temperature. This project produced empirical evidence for that effect, and further documented a simple model with predictive power over the artificial muscle fibers.

The robotic design portion of this project was simple, but it provided the author with an opportunity to develop a research tool that functioned like a potential application device, namely the antagonistic muscle fixture. While the fixture was never configured or operated in the full antagonistic configuration, it was used to collect empirical data that drove in-silico testing, and it could be easily re-used by a future researcher for similar testing. Design challenges in this project included test device integration, low-impact mechanical measurement, and unknown operating parameters of the muscle. The fixture's construction is extremely strong; it was designed to accommodate several muscles acting in parallel under high tension. Finite element analyses for critical parts, while omitted from this report for brevity, are included in the reference package design files.

In conclusion, the author wishes to thank the countless supporting parties to this work, and to reiterate that the technology treated herein holds promise for application in the field of soft robotics, and in a broad range of other technical fields. Twisted polymer artificial muscles are not without their limitations, but this low-cost, lightweight alternative to more traditional electromechanical actuators indicates an early step in the right direction for soft robotics actuation.

6 References

[1] "agonist muscle." *Taber's Medical Dictionary*. 2015. Retrieved from http://www.tabers.com/tabersonline/view/Tabers-Dictionary/765961/all/muscle

[2] C. Chou, B. Hannaford, Measurement and Modeliing of McKibben Pneumatic Artificial Muscles. *IEEE Trans. Robot. Auto.* **12** (1) 90-102 (1996).

[3] C. L. Choy, F. C. Chen, K. Young, Negative Thermal Expansion in Oriented Crystalline Polymers. *Jour. Poly. Sci. Poly. Phys. Ed.* **19** (2), 335-352 (1981).

[4] C. S. Haines *et al*., Supplementary Materials for Artificial Muscles from Fishing Line and Sewing Thread. *Science* **343**, 868 (2014). Supplementary Materials from *Science* online.

[5] C.S. Haines *et al*., Artificial muscles from fishing line and sewing thread. *Science* **343**, 868-872 (2014).

[6] C.S. Haines, *How to Make an Artificial Muscle Out of Fishing Line* (Science Friday, New York, 2014). Retrieved from http://www.sciencefriday.com/blogs/03/06/2014/how-to-make-an-artificial-muscle-out-of-fishing-line.html

[7] DARPA, *Upgraded Atlas robot to go wireless as the stakes are raised for the DARPA Robotics Challenge finals* (DARPA, Arlington, 2015). Retrieved from http://www.darpa.mil/NewsEvents/Releases/2015/01/20.aspx

[8] Dynalloy, *70°C and 90°C Flexinol® Actuator Wire Price Guide* (Dynalloy, Inc., Irvine, 2014). Retrieved from http://www.dynalloy.com/flexwire_70_90.php

[9] Dynalloy, *Technical Characteristics of Flexinol® Actuator Wire* (Dynalloy, Inc., Irvine, 2014). Retrieved from http://www.dynalloy.com/pdfs/TCF1140.pdf

[10] F. Daerden, D. Lefeber, B. Verrelst, R. Van Ham, Pleated pneumatic artificial muscles: actuators for automation and robotics. *Proc. 2011 IEEE/ASME Conf. Adv. Intelligent Mechatronics*, Como, Italy (2001).

[11] H. Herr, R. Kornbluh., New horizons for orthotic and prosthetic technology: artificial muscle for ambulation. *Proc. SPIE* **5385**, Smart Structures and Materials 2004: Electroactive Polymer Actuators and Devices (2004).

[12] H. Koerner, G. Price, N. A. Pearce, M. Alexander, R. A. Vaia, Remotely actuated polymer nanocomposites–stress-recovery of carbon-nanotube-filled thermoplastic elastomers. *Nat. Mat.* **3** 115-120 (2004).

[13] J. Cui *et al*., Combinatorial search of thermoelastic shape-memory alloys with extremely small hysteresis width. *Nat. Mat.* **5** 286-290 (2006).

[14] J. D. W. Madden *et al*., Artificial muscle technology: physical principles and naval prospects. *IEEE Jour. Ocean. Eng.* **29** (3) 706-728 (2004).

[15] J. Foroughi *et al.* Torsional carbon nanotube artificial muscles. *Science* **334** 494-497 (2011).

[16] J. L. Serres, thesis, Wright State University (2008).

[17] J. Leng, X. Lan, Y. Liu, S. Du, Shape-memory polymers and their composites: stimulus methods and applications. *Prog. Mat. Sci.* **56** 1077-1135 (2011).

[18] J. Yamaguchi, D. Nishino, A. Takanishi, Realization of dynamic biped walking varying joint stiffness using antagonistic driven joints. *Proc. 1998 IEEE Conf. Rob. Auto.*, Leuven, Belgium (1998).

[19] K. Hosoda, T. Takuma, A. Nakamoto, S. Hayashi, Biped robot design powered by antagonistic pneumatic actuators for multi-model locomotion. *Robotics and Autonomous Systems* **56**, 46-53 (2008).

[20] M. D. Lima *et al*. Electrically, chemically, and photonically powered torsional and tensile actuation of hybrid carbon nanotube yarn muscles. *Science* **338** 928-932 (2012).

[21] M.C. Yip, G. Niemeyer, High-Performance Robotic Muscles from Conductive Nylon Sewing Thread. *Proc. 2015 IEEE Conf. Rob. Auto.,* Seattle, Washington (2015).

[22] N. Li, C.S. Haines, M.D. Lima, M.J. de Andrade, S. Fang, J. Oh, M.E. Kozlov, F. Goktepe, O. Oktepe, D. Suh, R.H. Baughman, "Coiled and non-coiled twisted nanofiber yarn and polymer fiber torsional and tensile actuators," International Patent Application PCT/US2013/053227, Feb 6, 2014

[23] R. J. Maring, "Potentiometer mounting," U.S. Patent 2937861, May 24, 1960.

[24] R. Pelrine, R. Kornbluh, Q. Pei, J. Joseph, High-speed electrically actuated elastomers with strain greater than 100%. *Science* **287** 836-839 (2000).

[25] S. M. Mirvakili *et al*., Simple and strong: twisted silver painted nylon artificial muscle actuated by Joule heating. *Proc. SPIE* **9056**, Electroactive Polymer Actuatots and Devices (2014).

[26] Shadow Robot Company, *Air Muscle Hand* (Shadow Robot Company, London). Image provided by owner and used by express permission.

[27] Shadow Robot Company, *Shadow Dexterous Hand Technical Specification* (Shadow Robot Company, London, 2013). Retrieved from http://www.shadowrobot.com/wp-content/uploads/shadow_dexterous_hand_technical_specification_E1_20130101.pdf

[28] T. Chaulk, W. D. Hunt, J. Johnson, Dynamic Model of an Artificial Muscle Test Fixture. 2016, C-Term ME/RBE 4322, Worcester Polytechnic Institute. [Unpublished College Coursework].

[29] Y. Bar-Cohen, *Electroactive Polymer (EAP) Actuators as Artificial Muscles – Reality, Potential, and Challenges* (SPIE, Bellingham, ed. 2, 2004).

[30] Y. Kobayashi, A. Keller, The temperature coefficient of the c lattice parameter of polyethylene; an example of thermal shrinkage along the chain direction. *Polymer* **11** (2), 114-117 (1970).

APPENDIX A Antagonistic Stimulus Fixture Design Documents

The following pages contain mechanical specification drawings for the antagonistic figure. These drawings provide reference and replication information for the fixture provided to the Soft Robotics Laboratory at WPI.

PARTS LIST		
ITEM	QTY	PART NUMBER
1	1	EXTENSION SPRING - LEN 1 3/4 - OD 1/4 - WIRE 0.025
2	1	HEX NUT 6-32
3	4	HEX NUT 8-32
4	2	MCMASTER 60355K450
5	3	MCMASTER 93265A037
6	1	PAN HEAD SCREW 6 - 32 - 5/16
7	1	PAN HEAD SCREW 8 - 32 - 1
8	1	POTENTIOMETER SLIDER ARM
9	1	POTENTIOMETER SLIDER BASE
10	1	POTENTIOMETER SLIDER BUSHING
11	1	POTENTIOMETER SLIDER WASHER
12	1	ROTOR
13	2	ROTOR ROD - MCMASTER 8890K167 - CUT TO LENGTH AS NEEDED
14	1	SHAFT SPACER
15	2	SOCKET CAP SCREW 8 - 32 - 1 1/2
16	6	SOCKET CAP SCREW 8 -32 - 1 1/2
17	2	STATOR
18	2	STATOR ROD - MCMASTER 8890K167 - CUT TO LENGTH AS NEEDED
19	1	TORQUE RING ASSEMBLY
20	1	VISHAY 157-11103
21	1	VISHAY 157-11103 LOCK WASHER
22	1	VISHAY 157-11103 NUT

NOTES:
1. COMPONENT MATERIALS ARE SPECIFIED
   IN SUBCOMPONENT DRAWINGS
2. EQUIVALENT COMPONENTS MAY BE SUBSTITUTED
   FOR SPECIFIED COMMERCIAL, OFF-THE-SHELF ELEMENTS

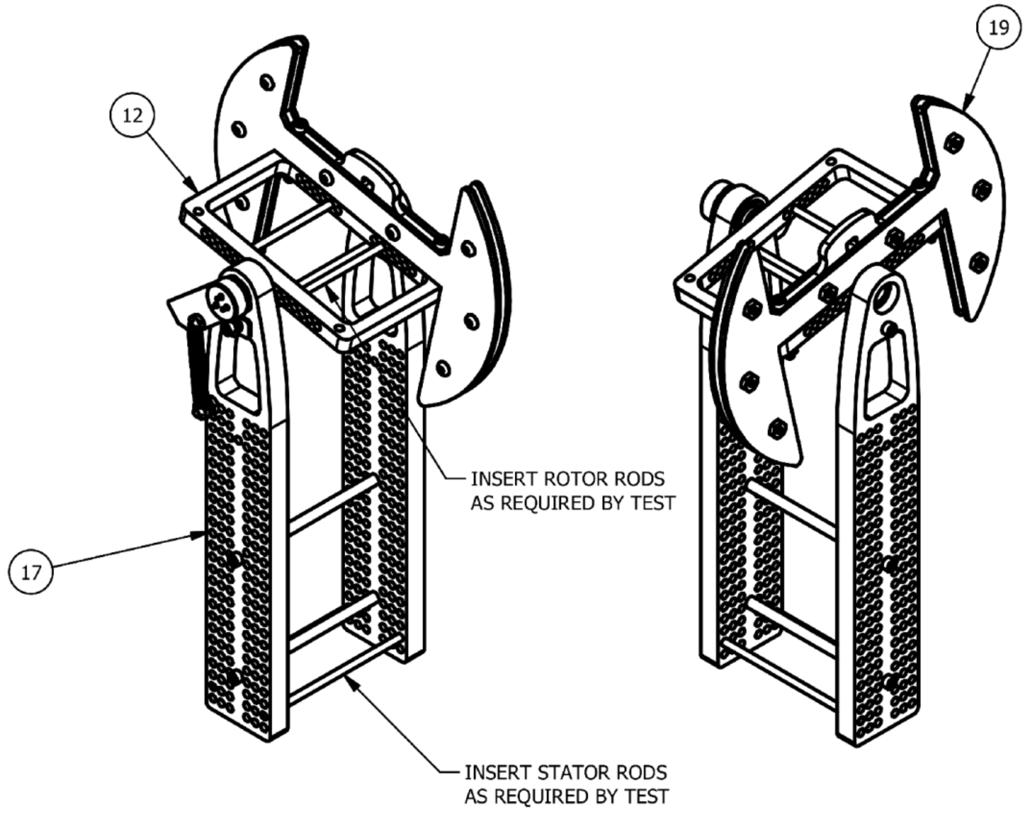
12
19
17
INSERT ROTOR RODS AS REQUIRED BY TEST
INSERT STATOR RODS AS REQUIRED BY TEST

DRAWN Bill Hunt	8/27/2015	SIZE A	DWG NO AssembledJoint
		SCALE 1/4	SHEET 1 OF 4
			REV

ASSEMBLY STEP ONE

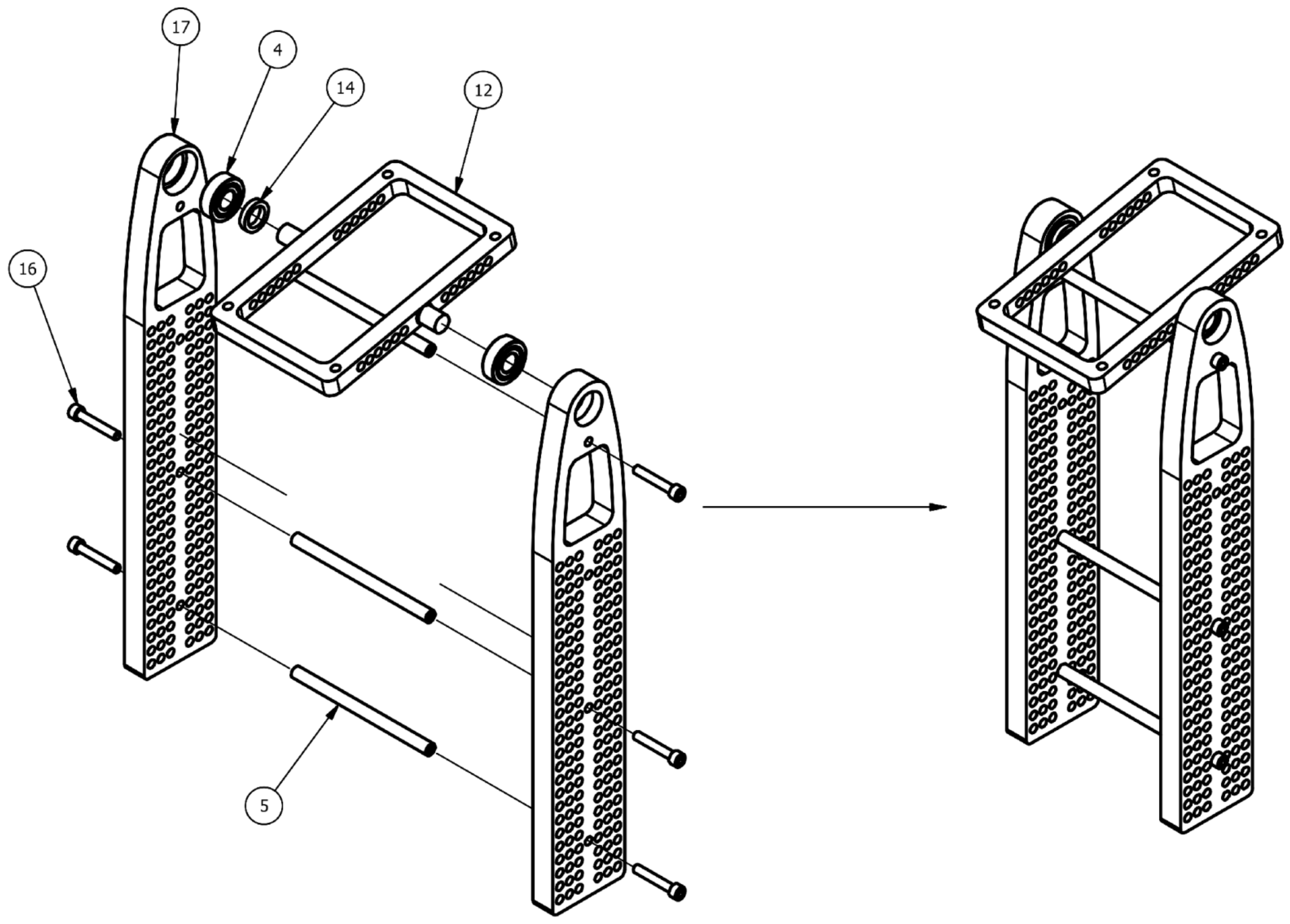

DRAWN Bill Hunt	8/27/2015	SIZE A	DWG NO AssembledJoint	REV
		SCALE 1/3		SHEET 2 OF 4

ASSEMBLY STEP TWO

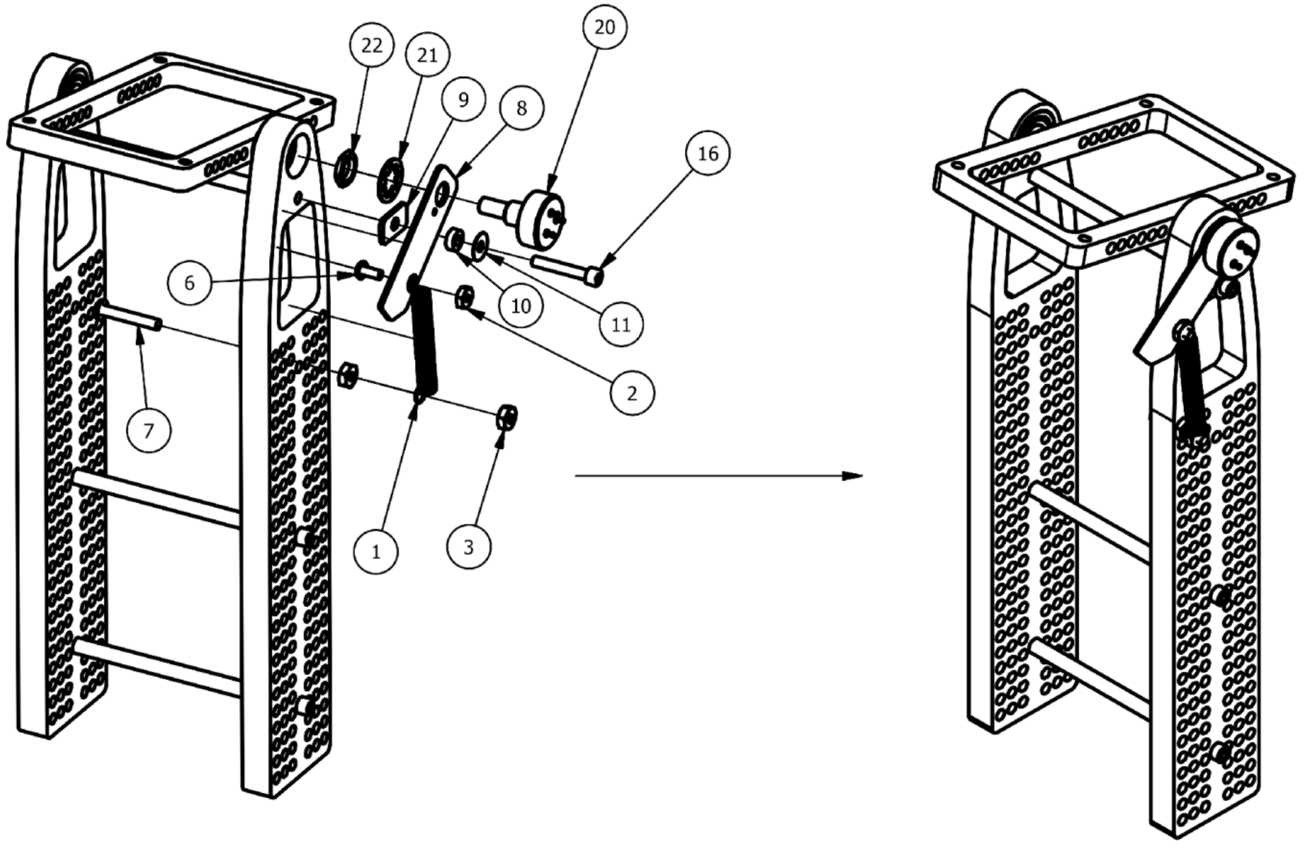

DRAWN Bill Hunt	8/27/2015	SIZE A		DWG NO AssembledJoint	REV
		SCALE 1/3		SHEET 3 OF 4	

ASSEMBLY STEP THREE

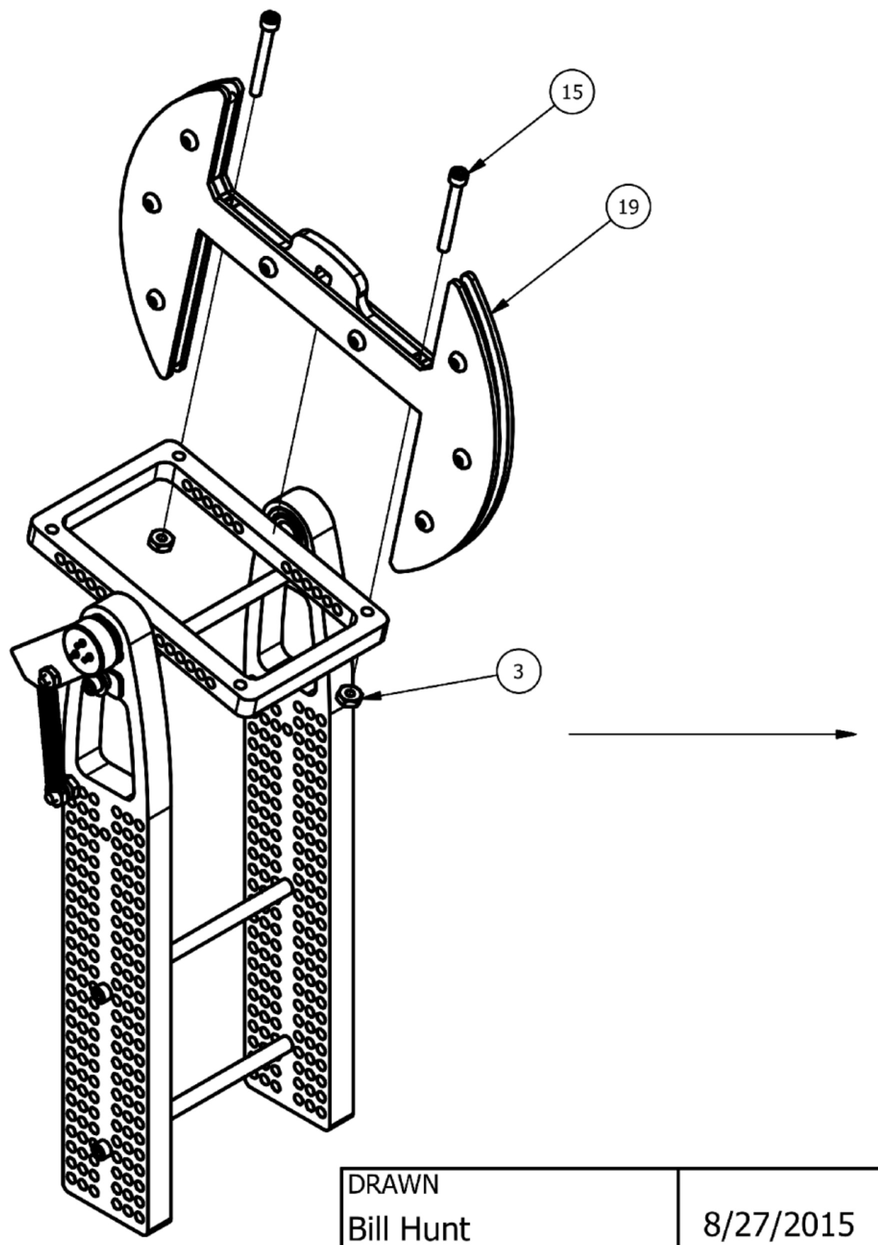

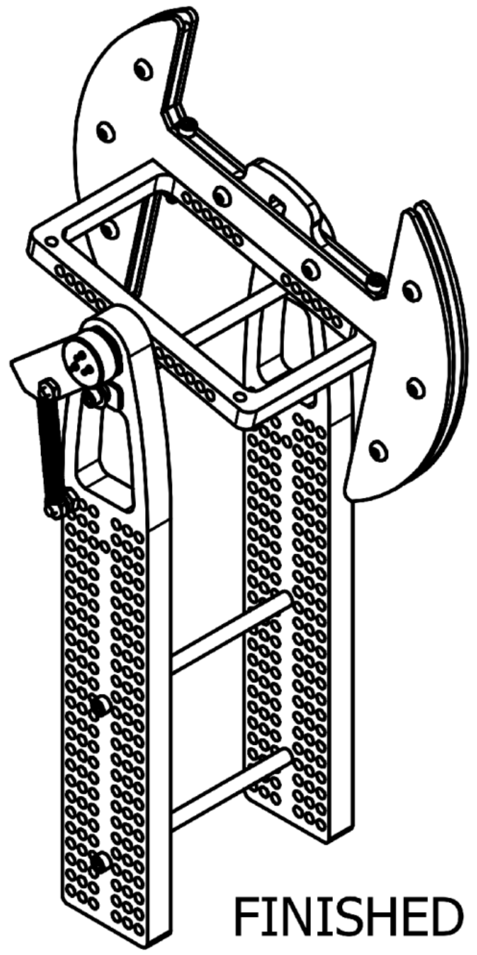

FINISHED ASSEMBLY

DRAWN Bill Hunt	8/27/2015	SIZE A	DWG NO AssembledJoint	REV
		SCALE 1/3		SHEET 4 OF 4

NOTES:
1. MATERIAL: ABS PLASTIC (UNLESS OTHERWISE NOTED)

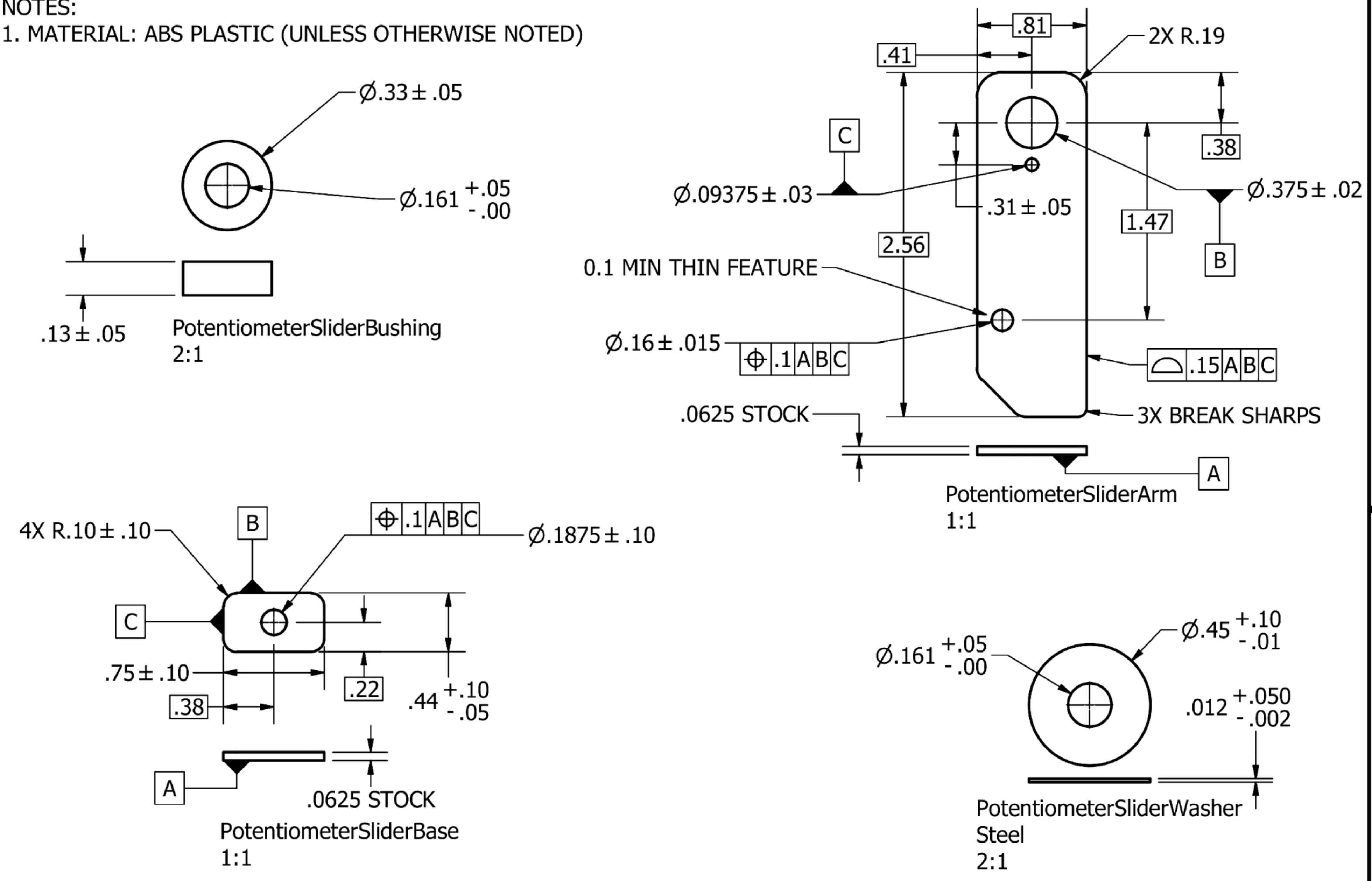

DRAWN Bill Hunt	8/27/2015	SIZE A	DWG NO Potentiometer Slider Elements	REV
		SCALE Varies		SHEET 1 OF 1

NOTES:
1. MATERIAL: ALUMINUM

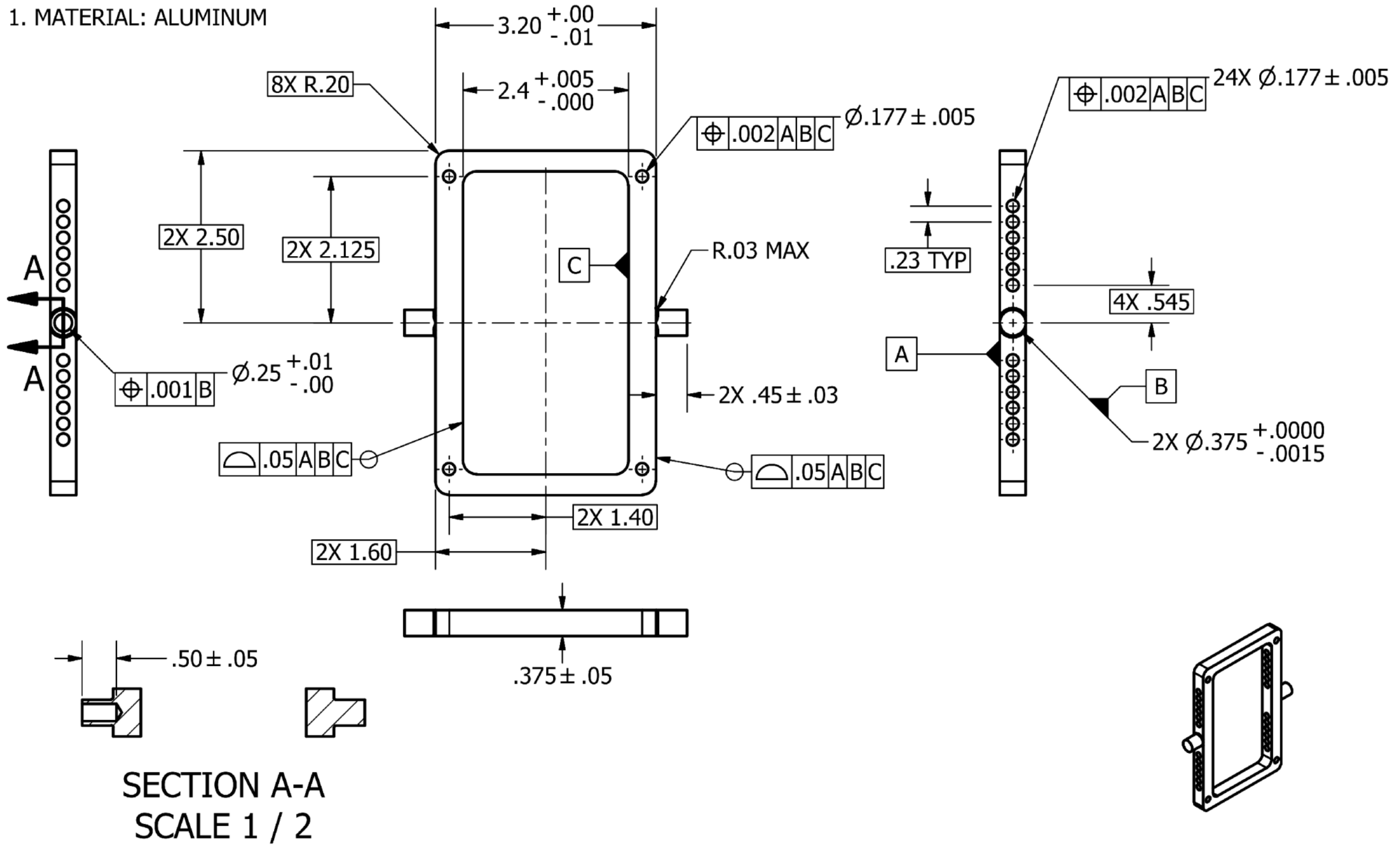

DRAWN		SIZE	DWG NO	REV
Bill Hunt	8/23/2015	A	Rotor	
		SCALE 1/2	SHEET 1 OF 1	

NOTES:
1. MATERIAL: ACRYLIC

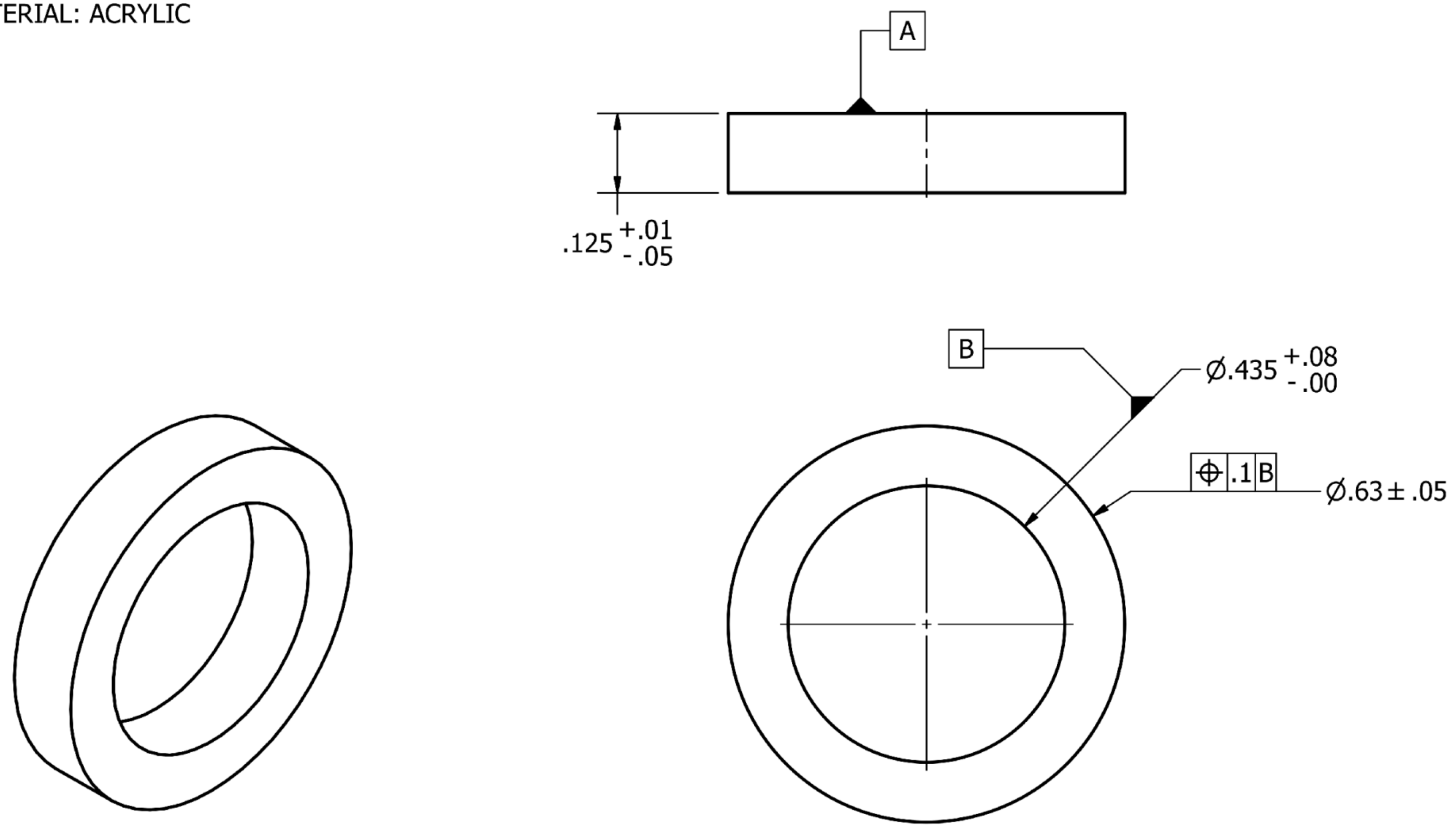

DRAWN Bill Hunt	8/27/2015	SIZE A	DWG NO ShaftSpacer	REV
		SCALE 4:1		SHEET 1 OF 1

NOTES:
1. MATERIAL: ALUMINUM

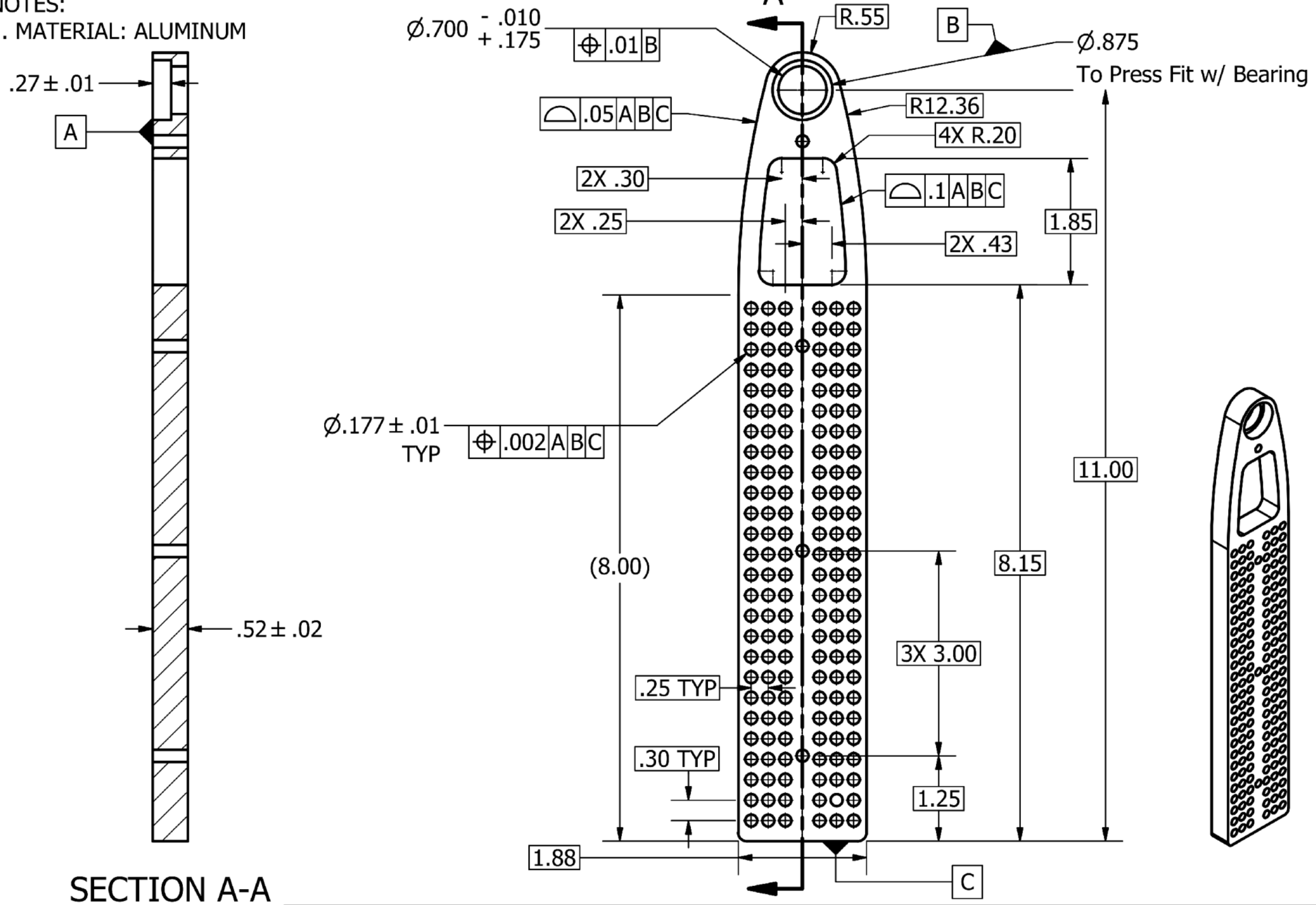

SECTION A-A
SCALE 1/2

DRAWN Bill Hunt	8/27/2015	SIZE A	DWG NO Stator	REV
		SCALE 1/2		SHEET 1 OF 1

NOTES:
1. MATERIAL: LASER CUT ACRYLIC

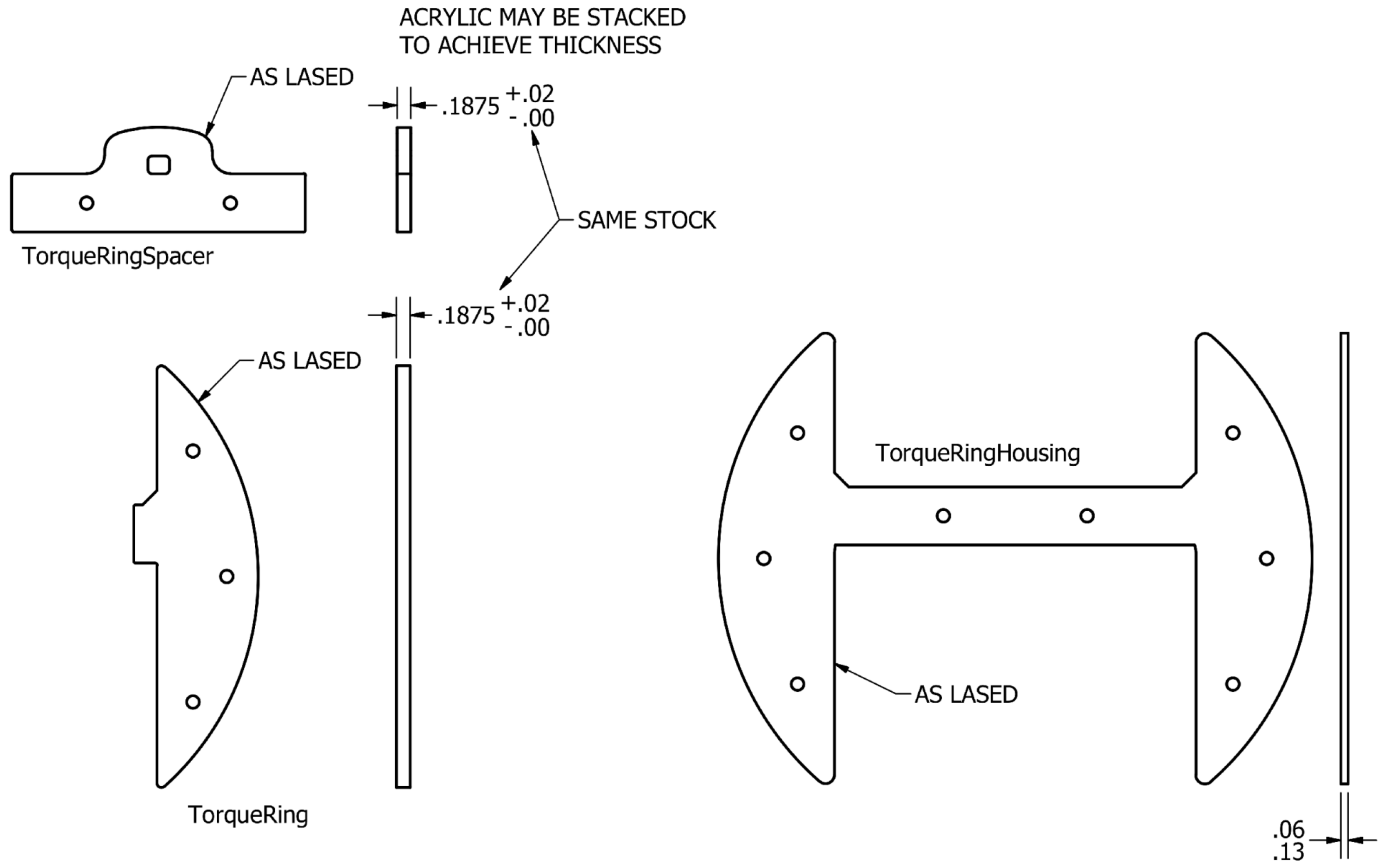

DRAWN Bill Hunt	8/27/2015	SIZE A	DWG NO Torque Ring Items	REV
		SCALE 1/2		SHEET 1 OF 1

PARTS LIST		
ITEM	QTY	PART NUMBER
1	8	BUTTON HEAD SCREW 8 - 32 - 1/2
2	8	HEX NUT 8-32
3	2	TORQUE RING
4	2	TORQUE RING HOUSING
5	1	TORQUE RING SPACER

NOTES:
1. COMPONENT MATERIALS ARE SPECIFIED IN SUBCOMPONENT DRAWINGS

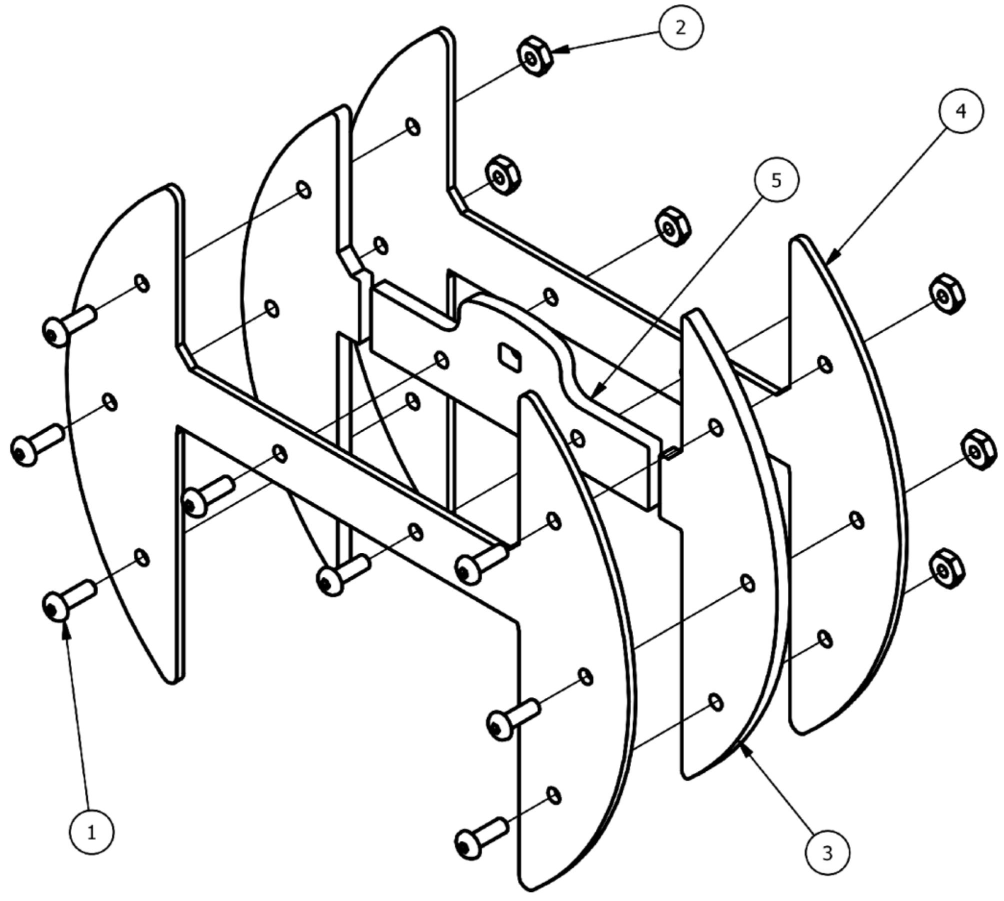

ASSEMBLY STEP

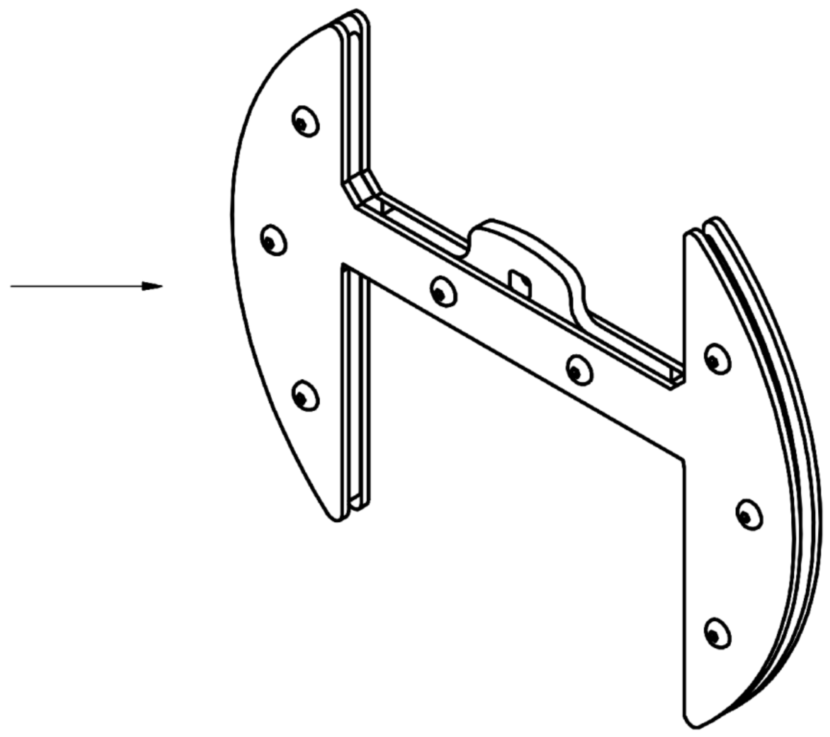

FINISHED ASSEMBLY

DRAWN Bill Hunt	8/27/2015	SIZE A	DWG NO Torque Ring Assembly	REV
		SCALE 1/4		SHEET 1 OF 1

APPENDIX B ANTAGONISTIC STIMULUS FIXTURE SOFTWARE

This appendix lists the primary source code files necessary for the operation of the antagonistic test fixture. Note that additional simple scripts were also created, using the same libraries, to facilitate tests without temperature stimuli, and calibration runs. An older, single channel version of the antagonistic test script was also used for tubular heater control. These ancillary scripts are omitted from this report for brevity, but all test scripts from this project are in custody of the WPI Soft Robotics Laboratory, c/o Prof. Cagdas Onal. As noted previously, this project did not use any source control repository or formal versioning, because the number of software tools developed was so small.

Source and license information is provided for each program, under its header. All *.ino programs are intended to execute on the Arduino Duemilanove or Uno board, and all *.py programs and modules are designed to execute under Python 2.7.10 32-bit.

License Text – MIT License (See notes about granular application)

Arduino Interface Program – prototype/prototype.ino

```
#ifndef SERIAL_RATE
#define SERIAL_RATE         115200
#endif

#ifndef SERIAL_TIMEOUT
#define SERIAL_TIMEOUT      5
```

```
#endif

void setup() {
    Serial.begin(SERIAL_RATE);
    Serial.setTimeout(SERIAL_TIMEOUT);
}

void loop() {

    int pin = 0;

    switch (readData()) {
        case 0 :
            //set digital low
            //set digital high
            pin = readData();
            pinMode(pin, OUTPUT);
            digitalWrite(pin, LOW); break;
        case 1 :
            //set digital high
            pin = readData();
            pinMode(pin, OUTPUT);
            digitalWrite(pin, HIGH); break;
        case 2 :
            //get digital value
            Serial.println(digitalRead(readData())); break;
        case 3 :
            // set analog value
            pin = readData();
            pinMode(pin, OUTPUT);
            analogWrite(pin, readData()); break;
        case 4 :
            //read analog value
            Serial.println(analogRead(readData())); break;
        case 99:
            //just dummy to cancel the current read, needed to prevent lock
            //when the PC side dropped the "w" that we sent
            break;
    }
}

char readData() {
    Serial.println("w");
    while(1) {
        if(Serial.available() > 0) {
            return Serial.parseInt();
        }
    }
}
```

Arduino Prototyping Interface Script – arduino.py

```
#!/usr/bin/env python
# -*- coding: utf-8 -*-

import serial
import time

class Arduino(object):

    def __init__(self, port, baudrate=115200):
        self.serial = serial.Serial(port, baudrate, timeout=1)
        self.serial.write(b'99')

    def __str__(self):
        return "Arduino is on port %s at %d baudrate" %(self.serial.port, self.serial.baudrate)

    def setLow(self, pin):
        self.__sendData('0')
        self.__sendData(pin)
        return True
    def setHigh(self, pin):
        self.__sendData('1')
        self.__sendData(pin)
        return True

    def getState(self, pin):
        self.__sendData('2')
        self.__sendData(pin)
        return self.__formatPinState(self.__getData()[0])

    def analogWrite(self, pin, value):
        self.__sendData('3')
        self.__sendData(pin)
        self.__sendData(int(value))
        return True

    def analogRead(self, pin):
        self.__sendData('4')
        self.__sendData(pin)
        return self.__getData()

    def __sendData(self, serial_data):
        while(self.__getData()[0] != "w"):
            pass
        serial_data = str(serial_data).encode('utf-8')
        self.serial.write(serial_data)

    def __getData(self):
        input_string = self.serial.readline()
        if input_string is None:
            return "\n"
        else:
            input_string = input_string.decode('utf-8')
            return input_string.rstrip('\n')

    def __formatPinState(self, pinValue):
        if pinValue == '1':
            return True
        else:
            return False

    def close(self):
        self.serial.close()
        return True
```

AMPROBE TMD-56 Interface Module Script – amprobe.py (See notes about granular license application)

```
# This source is based on code from the artisan-roaster-scope project at https://github.com/artisan-
roaster-scope/artisan
# The artisan-roaster-scope project is licensed under GPL v3. To comply with the terms of that license,
GPL v3 applies granularly
# to this file. Note that the GPL v3 does not apply to the other files in the Polymer Muscle MQP
project, INCLUDING THE PROJECT REPORT IN WHICH COPIES OF THE LICENSED FILES HAVE BEEN EMBEDDED, unless
otherwise specified.

# This program provides an interface to the Amprobe TMD-56 thermocouple meter T1 and T2 in Python

# REQUIREMENTS
# python
# pyserial

import serial
import time
import binascii
from threading import Thread, Lock


class AmprobeMeter:
    __stableT1 = 0
    __stableT2 = 0
    port = ''
    __thread = None
    __lock = None

    def __init__(self, port):
        self.port = port
        self.__lock = Lock()
        self.__thread = Thread(target=self.__readMeter)
        self.__thread.daemon = 1
        self.__thread.start()

    def getTemperatures(self):
        with self.__lock:
            return self.__stableT1, self.__stableT2


    def __readMeter(self):
        while(self.__thread.isAlive()):
            try:
                ser = serial.Serial(self.port, baudrate=19200, bytesize=8, parity='E', stopbits=1,
timeout=1)
                command = "#0A0000NA2\r\n"
                ser.write(command)
                r = ser.read(14)
                ser.close()

                #convert to binary to hex string
                s1 = binascii.hexlify(r[5] + r[6])
                s2 = binascii.hexlify(r[10]+ r[11])

                #we convert the strings to integers. Divide by 10.0 (decimal position)
                t1 = int(s1,16)/10.
                t2 = int(s2,16)/10.

                with self.__lock:
                    self.__stableT1 = t1
                    self.__stableT2 = t2

            except serial.SerialException, e:
                print e
```

Temperature Control, Test and Logging Script – tempTest.py

```
import amprobe
import time
import datetime
import arduino
from threading import Thread, Lock

class TempController:
    __arduinoA = None
    __arduinoB = None
    __meter = None
    __pinA = 0
    __pinB = 0
    __thread = None
    __outputThread = None
    __prevUpdateTime = 0
    __period = 0
    __mainThreadLock = None
    __outputThreadLock = None
    __enabled = 0
    __currentOutputA = 0
    __currentOutputB = 0
    __setpointA = 0
    __setpointB = 0
    __kC = 0
    __kF = 0
    __kP = 0
    __kI = 0
    __ILimit = 0
    __accumulatorA = 0
    __accumulatorB = 0
    __prevUnstableTimeA = 0
    __prevUnstableTimeB = 0
    __tempStableA = 0
    __tempStableB = 0
    __controlScale = 0.55

    __temperatureUpdate = 0
    __currentTemperatureA = 0
    __currentTemperatureB = 0
    __prevTemperatureA = 0
    __prevTemperatureB = 0
    __temperatureSteadyTime = 10
    __tempThresh = 1.0

    def __init__(self, arduinoAPort, arduinoBPort, amprobePort, temperaturePinA, temperaturePinB, 
updatePeriod,\
                 kC, kF, kP, kI, accumLimit, logFileName):
        self.__arduinoA = arduino.Arduino(arduinoAPort)
        self.__arduinoB = arduino.Arduino(arduinoBPort)
        time.sleep(1)
        self.__meter = amprobe.AmprobeMeter(amprobePort)
        self.__pinA = temperaturePinA
        self.__pinB = temperaturePinB
        self.__period = updatePeriod
        self.__prevUpdateTimeA = time.time()
        self.__prevUpdateTimeB = self.__prevUpdateTimeA
        self.__prevUnstableTimeA = self.__prevUpdateTimeA
        self.__prevUnstableTimeB = self.__prevUpdateTimeB
        self.__kC = kC
        self.__kF = kF
        self.__kP = kP
        self.__kI = kI
        self.__ILimit = accumLimit
        self.__logFile = open(logFileName, 'w')

        self.__mainThreadLock = Lock()
        self.__mainThread = Thread(target=self.__updateController)
        self.__mainThread.daemon = 1
        self.__mainThread.start()

        self.__outputThreadLock = Lock()
        self.__outputThread = Thread(target=self.__writeToOutput)
        self.__outputThread.daemon = 1
        self.__outputThread.start()


    def setEnabled(self, enabled):
        with self.__mainThreadLock:
            self.__enabled = enabled

            # turn on LED if controller is enabled
            # turn off LED and heater if controller is disabled
            if enabled:
                header="Time (s), Temperature A (C), Setpoint A (C), Temperature Stable A, Temperature B 
(C), Setpoint B (C), Temperature Stable B, Temperature Update, Potentiometer Reading"
                print header
                self.__logFile.write(header + '\n')
                self.__arduinoA.setHigh(13)
            else:
                time.sleep(0.5)
                self.__arduinoA.setLow(13)

                with self.__outputThreadLock:
                    self.__arduinoB.analogWrite(self.__pinA, 0)
                    self.__arduinoB.analogWrite(self.__pinB, 0)

    def setSetpoint(self, setpointA, setpointB):
        with self.__mainThreadLock:
            self.__temperatureUpdate = 1
            self.__setpointA = setpointA
            self.__setpointB = setpointB

            self.__tempStable = 0

    def stableTemperatureA(self):
        with self.__mainThreadLock:
            return self.__tempStableA

    def stableTemperatureB(self):
        with self.__mainThreadLock:
            return self.__tempStableB

    def __updateController(self):
        while self.__mainThread.isAlive():
            currentTime = time.time()
            if currentTime - self.__prevUpdateTime >= self.__period:
                self.__prevUpdateTime = currentTime

                # update temperature
                # get thread-safe copies
                with self.__mainThreadLock:
                    self.__prevTemperatureA = self.__currentTemperatureA
                    self.__prevTemperatureB = self.__currentTemperatureB
                    self.__currentTemperatureA = self.__meter.getTemperatures()[0]
                    self.__currentTemperatureB = self.__meter.getTemperatures()[1]

                    if self.__currentTemperatureA > self.__setpointA + self.__tempThresh or
self.__currentTemperatureA < self.__setpointA - self.__tempThresh:
                        self.__prevUnstableTimeA = currentTime

                    if self.__currentTemperatureB > self.__setpointB + self.__tempThresh or
self.__currentTemperatureB < self.__setpointB - self.__tempThresh:
                        self.__prevUnstableTimeB = currentTime

                    self.__tempStableA = (currentTime - self.__prevUnstableTimeA) >
self.__temperatureSteadyTime
                    self.__tempStableB = True# Channel B is disabled (currentTime -
self.__prevUnstableTimeB) > self.__temperatureSteadyTime

                    localEnabled = self.__enabled

                    localSetpointA = self.__setpointA
                    localStableA = self.__tempStableA
                    localSetpointB = self.__setpointB
                    localStableB = self.__tempStableB

                    localTemperatureUpdate = self.__temperatureUpdate
                    self.__temperatureUpdate = 0

                if localEnabled:
                    errorA = localSetpointA - self.__currentTemperatureA
                    errorB = localSetpointB - self.__currentTemperatureB

                    # compute integral state
                    self.__accumulatorA += errorA * (currentTime - self.__prevUpdateTime)
                    if self.__accumulatorA > self.__ILimit:
                        self.__accumulatorA = self.__ILimit
                    elif self.__accumulatorA < -self.__ILimit:
                        self.__accumulatorA = -self.__ILimit

                    self.__accumulatorB += errorB * (currentTime - self.__prevUpdateTime)
                    if self.__accumulatorB > self.__ILimit:
                        self.__accumulatorB = self.__ILimit
                    elif self.__accumulatorB < -self.__ILimit:
                        self.__accumulatorB = -self.__ILimit

                    # compute output
                    outputA = self.__controlScale*(self.__kC + self.__kF*localSetpointA + 
self.__kP*errorA + self.__kI*self.__accumulatorA)
                    if outputA>255:
                        outputA = 255
                    elif outputA<0:
                        outputA = 0

                    outputB = self.__controlScale*(self.__kC + self.__kF*localSetpointB + 
self.__kP*errorB + self.__kI*self.__accumulatorB)
                    if outputB>255:
                        outputB = 255
                    elif outputB<0:
                        outputB = 0

                    with self.__mainThreadLock:
                        self.__currentOutputA = outputA
                        self.__currentOutputB = outputB

                    position = self.__arduinoA.analogRead(0)

                    logString = str(currentTime) + "," + str(self.__currentTemperatureA) + "," + 
str(localSetpointA) + "," + str(localStableA) + "," + str(self.__currentTemperatureB) + "," + 
str(localSetpointB) + "," + str(localStableB) + "," + str(localTemperatureUpdate)+ "," + position
                    print logString
                    self.__logFile.write(logString)

    def __writeToOutput(self):
        while self.__outputThread.isAlive():
            with self.__mainThreadLock:
                outputA = self.__currentOutputA
                outputB = 0# Channel B is disabled self.__currentOutputB

            with self.__outputThreadLock:
                self.__arduinoB.analogWrite(self.__pinA, self.__currentOutputA)
                self.__arduinoB.analogWrite(self.__pinB, self.__currentOutputB)

            time.sleep(0.1)


# List temperature setpoints here
# Both channel lists must specify the same number of temperature setpoints
temperaturesA = [25,90,25,90]
temperaturesB = [25,90,25,90]

try:
    time.sleep(1)
    filename = raw_input("Enter a log file name: ")
    timeInterval = 0.03
    controller = TempController("COM4", "COM6", "COM8", 6, 5, timeInterval, kC=-55.4, kF=1.5, kP=30, 
kI=timeInterval*25.0, accumLimit=500, logFileName = "Log - " + datetime.datetime.today().strftime("%a 
%d-%m-%Y %H-%M-%S") + " - " + filename)

    controller.setEnabled(1)
    for i in range(len(temperaturesA)):
        controller.setSetpoint(temperaturesA[i],temperaturesB[i])
        while not (controller.stableTemperatureA() and controller.stableTemperatureB()):
            time.sleep(0.1)
        raw_input()

    print "Stopping test...\n\n"
    controller.setEnabled(0)
    print "Controller disabled.\n\n"


except KeyboardInterrupt:
    print "Stopping test...\n\n"
    controller.setEnabled(0)
    print "Controller disabled.\n\n"
```

APPENDIX C ANTAGONISTIC STIMULUS FIXTURE OPERATING INSTRUCTIONS

Operating the antagonistic test fixture is straightforward. Fig. 10 (in section 3.3) shows the proper electrical and data-line configuration for the fixture. If an existing test script is to be used, that script will generally need to be modified slightly to suit the test at hand. For example, the names of COM ports and the lists of temperature set points may need to be changed. The scripts provided with the fixture are all very simple utility programs less than 500 lines. Detailed documentation of test script design is omitted, as it is assumed that any user of the fixture is well-versed in Python programming.

These instructions assumed that the user has already configured or custom-designed a test script for their intended use of the fixture, and now seeks to execute a physical test using the fixture proper.

The antagonistic test fixture may be configured in a purely antagonistic arrangement (two muscles antagonizing each other, with an optional spring or weight bias), a "dummy" antagonistic arrangement (one muscle fighting a spring or weight bias), or a purely dynamical arrangement (a combination of springs and weights that includes no muscle fibers).

The purely dynamical arrangement is convenient for fixture calibration, and requires no muscle setup. Springs may be strung between fixturing pins, or bolted to the fixture body as convenient. Bias weights may be suspended from the plastic torque application disk using string or monofilament. A tie-off point of the suspension element has been included in the design of the torque application disk for this purpose.

When a bias weight of more than a few grams is applied, it is necessary to clamp the fixture to a solid work surface to prevent tipping. A *DeWALT* brand sliding clamp has been included with the fixture for this purpose; the clamp's wide mouth permits various modes of fixturing as convenient.

The processes for setting up the purely antagonistic arrangement and dummy antagonistic arrangement are identical. The bias weight or springs may be affixed to the fixture just as in the purely dynamical arrangement, but a defined procedure must be followed in order to properly affix the muscles to the fixture:

1. Insert a fixture pin (STATOR ROD in Appendix A) into the selected muscle mounting hole on either stator plate.
2. Slide a heater tube onto the sample two-ply muscle fiber.
3. Grasp the exposed bottom end (without the aluminum crimp) of the two-ply muscle fiber in two locations. Twist the fiber in a direction opposite the direction of ply. This will cause the ply to unwind temporarily, creating a gap between two singleton muscle fibers.
4. Insert the end of the fixture pin into the gap formed in the muscle, then allow the muscle to relax. At this point, the heater tube should be captured between the crimped end of the muscle fiber and the bulge created by the infiltrating fixture pin.
5. Gently draw the pin along the muscle's length until it rests at one end of the muscle, adjacent to the terminal loop of fiber. Center the pin on the fixture body, inserting it into the second stator plate. At this point, the position of the muscle on the fixture pin may be adjusted if necessary.
6. Allow the muscle to relax torsionally, then obtain a dummy fixture pin (any unused STATOR ROD or ROTOR ROD will do).
7. Insert the dummy fixture pin into the dangling end of the muscle using the same method just applied with the stator pin, and gently draw it to the end of the fiber (adjacent to the metal crimp).
8. Obtain a fixture pin for the rotor (ROTOR ROD in Appendix A), and insert it into the selected muscle mounting hole on the rotor.
9. Rotate the dummy pin (which remains inserted in the dangling end of the muscle) until there is no torsional strain in the muscle fiber.

10. Align the end of the dummy pin with the rotor fixture pin. In most cases, the dummy pin will not come to rest perfectly in parallel with the fixture pin axis. Rotate the dummy pin the minimum amount necessary to align it closely with the fixture pin, then slide the muscle off the dummy pin and onto the rotor fixture pin. The goal is to transfer the muscle from the dummy pin to the fixture pin with minimal introduction of twist.

The steps above may be applied for an arbitrary number of muscles. Multiple muscles may be strung to the same fixture pin(s), and multiple sets of fixture pins may be installed in the fixture as dictated by the test.